Chem Soc Rev

REVIEW ARTICLE

View Article Online
View Journal | View Issue

Cite this: *Chem. Soc. Rev.*, 2023, 52, 6554

Label-free optical biosensing: going beyond the limits

Andrei V. Kabashin *[a] Vasyl G. Kravets [b] and Alexander N. Grigorenko *[b]

Label-free optical biosensing holds great promise for a variety of applications in biomedical diagnostics, environmental and food safety, and security. It is already used as a key tool in the investigation of biomolecular binding events and reaction constants in real time and offers further potential additional functionalities and low-cost designs. However, the sensitivity of this technology does not match the routinely used but expensive and slow labelling methods. Therefore, label-free optical biosensing remains predominantly a research tool. Here we discuss how one can go beyond the limits of detection provided by standard optical biosensing platforms and achieve a sensitivity of label-free biosensing that is superior to labelling methods. To this end we review newly emerging optical implementations that overcome current sensitivity barriers by employing novel structural architectures, artificial materials (metamaterials and hetero-metastructures) and using phase of light as a sensing parameter. Furthermore, we elucidate the mechanism of plasmonic phase biosensing and review hyper-sensitive transducers, which can achieve detection limits at the single molecule level (less than 1 fg mm^{-2}) and make it possible to detect analytes at several orders of magnitude lower concentrations than so far reported in literature. We finally discuss newly emerging layouts based on dielectric nanomaterials, bound states in continuum, and exceptional points.

Received 2nd March 2023

DOI: 10.1039/d3cs00155e

rsc.li/chem-soc-rev

[a] *Aix Marseille Université, CNRS, UMR 7341 CNRS, LP3, Campus de Luminy-case 917, 13288, Marseille Cedex 9, France. E-mail: andrei.kabashin@univ-amu.fr*
[b] *School of Physics and Astronomy, University of Manchester, Manchester, M13 9PL, UK. E-mail: Vasyl.Kravets@manchester.ac.uk, Alexander.Grigorenko@manchester.ac.uk*

Andrei V. Kabashin

Andrei V. Kabashin is a Research Director (DR1) of the French National Center of Scientific Research (CNRS), affiliated to LP3 institute of Aix-Marseille University, Marseille, France. He was awarded MPhys degree (1989) from the Moscow Institute of Physics and Technology and a PhD degree (1994) from A. M. Prokhorov General Physics Institute, Moscow, Russia. Before 2009, he worked as a Research Professor in Ecole Polytechnique de Montreal at the University of Montreal, Montreal, Canada. His research interests include the development of artificial materials for ultrasensitive biosensing, plasmonics, laser-ablative synthesis and characterization of nanomaterials for biomedical and energy applications.

Vasyl G. Kravets

Vasyl G. Kravets received his PhD degree in physics (1990) from Taras Shevchenko University, Kiev, Ukraine. He worked in the Institute for Information Recording, NAS, Kiev, Ukraine, as a post-doctoral research scientist and later as a postdoctoral research fellow, University of York, UK, and an invited research scientist, University of Duisburg, Germany. He is currently a Research Fellow in the plasmonic group of Prof. A. Grigorenko in Department of Physics and Astronomy, the University of Manchester, UK. His current research interest focuses on development of hybrid plasmonic-two-dimensional nanostructures and their applications in bio- and medical sensing, plasmonically coupled optoelectronic devices and the solar photovoltaics field.

1. Introduction

Biosensors are designed to monitor and analyze affinity-binding interactions between a target analyte from biological samples (*e.g.*, antigen, protein, peptide, DNA, RNA segments) and its selective receptor immobilized on a surface (*e.g.*, antibody, protein, peptide, *etc.*). Biosensors present the key element in many tasks of biomedical diagnostics, such as the detection of biomarkers of infections, cancer diagnosis, cardio control, immune status, and rational drug design, as well as environmental and food safety, security and doping screening.[1–4] Conventional biosensing is based on the use of fluorescence or radio labels to detect bio-molecular binding, but the labelling step necessitates extra time, increases cost and can lead to a false negative signal by occluding the binding site.[1,3] An alternative label-free approach is based on optical transduction. Since the optical refractive index (RI) of most biological molecules is greater than that of water (1.45–1.55 compared to 1.33 Refractive Index Units (RIU), respectively), an increase of the thickness of a biological layer due to binding is accompanied by a change of RI of a thin surface layer (typically between a few nm and tens of nm). Optical biosensors are designed to sensitively control RI variations in this layer, which allows one to not only avoid the use of labels, but also characterize biomolecular interactions in real time, thus obtaining information on kinetic constants of the reactions.[1]

Despite the existence of several optical biosensing schemes, including interferometry,[5] resonant mirrors,[6] waveguides,[7] total internal reflection,[8] and whispering gallery modes,[9] plasmonic biosensing is so far the most successful and popular technology for label-free detection and characterization of biomolecular interactions.[10–15] Plasmonic biosensors employ surface plasmons, or collective oscillations of free electrons in metal,[16] which are optically excited at the interface of a noble metal (gold) and a liquid medium. Plasmon excitation leads to a strong enhancement of the electric field near the metal, such that it penetrates the liquid medium to a depth ranging from 30 nm to 200 nm, which makes plasmons very sensitive to local RI changes. Based on the excitation of propagating surface plasmon polaritons in thin gold films,[10,11] surface plasmon resonance (SPR) forms the core of plasmonic biosensing technology. An extension of SPR, called localized plasmon resonance (LPR), uses metallic nanostructures[15,17,18] and brings about a number of new functionalities, including compatibility with modern biomolecular nano-architectures, size selectivity and spectral tuneability, as well as an additional surface enhanced Raman scattering (SERS) sensing channel. However, despite the proven success of optical biosensing in plasmonic and alternative implementations[12–15,17–22] and its application in many biomedical, environmental, food quality and other tasks, this technology remains a research tool, not used in hospitals or homes. The main bottleneck is related to 1–2 orders of magnitude lower sensitivity of label-free transducers compared to label-based counterparts, which is related to structural limitations of the biosensor architectures and the use of amplitude-sensitive parameters for data acquisition (angular or spectral position of the plasmonic resonance extracted from light intensity).[12–14,18]

Here we review newly-emerging approaches to radically enhance optical sensor transducers and thus overcome the sensitivity limit of current label-free biosensing platforms, see Fig. 1. From the many existing options, we have selected only those that can be deployed *en masse* and could challenge ubiquitous labelling methods. These include new emerging structures, new materials, and new phenomena that can be used to radically advance label-free biosensing (Fig. 1). It is clear that these three options are interconnected: new structures (periodic and aperiodic) give directions for the design of novel materials in order to open up access to the implementation of novel optical phenomena that enable much-improved sensitivity going well beyond current detection limits. As examples,

Alexander N. Grigorenko

Alexander Grigorenko is a Professor of Physics at the Department of Physics and Astronomy at Manchester University, UK. He leads a nano-optics lab which studies light-matter interactions at the nanoscale. He was awarded MPhys (1986) and PhD (1989) degrees by the Moscow Institute of Physics and Technology. Before Manchester, he worked as a senior researcher at the A.M. Prokhorov General Physics Institute, Moscow, Russia, and as PDRA at Bath and Plymouth Universities, UK. His research interests include optics, plasmonics, hybrid 2D materials, magnetism, superconductivity, and photochemistry.

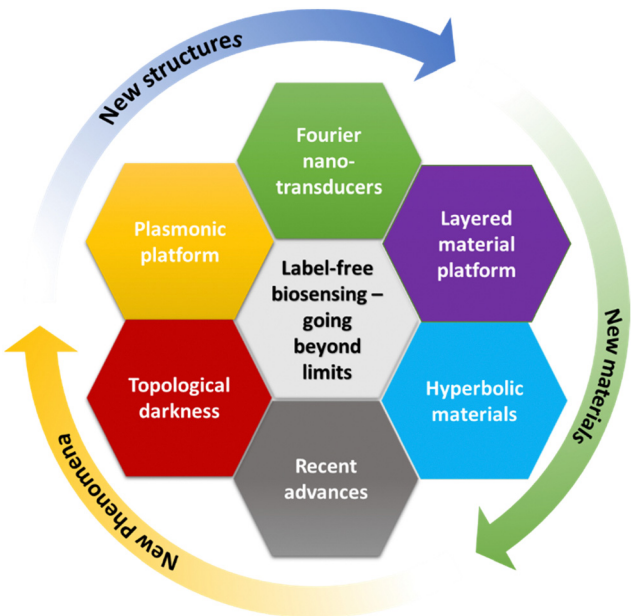

Fig. 1 Scope of label-free optical biosensing covered in this review.

new structures include coupled plasmonic structures, topologically dark heterostructures and layered structures, Fourier nanotransducers, while new materials include hyperbolic metamaterials, hybrid plasmonic-2D metasurfaces and 3D plasmonic metamaterials. We will discuss strong progress achieved in dielectric and plasmonic biosensing platforms, amplitude and phase readout schemes, as well as recent advances connected to emerging phenomena such as topological darkness, bound states in continuum and exceptional points, Goos–Hänchen effect, *etc.* Sensor transducers employing optical phase as the sensing parameter will form one of main focuses of this review. These transducers promise a breakthrough solution for the bottleneck sensitivity problem due to the singular (jump-like) behaviour of the optical phase at points of a sudden drop in light intensity (light darkness) owing to its ambiguity at the zero value of system parameters.[23,24] The detection sensitivity in this case is determined by the jump's sharpness,[25–29] allowing for virtually unlimited sensitivity.

Combined with simplicity of analysis, rapid detection times and the relatively low cost of optical label-free detection, these new implementations of biosensing could be especially important for the diagnosis of dangerous diseases and the detection of deadly pathogens and could be used to fight pandemics or perform population screening.

2. Label-free optical biosensors: comparison of sensitivities of different transducers and interrogation methods

As mentioned above, propagating surface plasmon polaritons, SPR technique,[10–14,22] and localised plasmons, LPR technique,[15,18] form the core of conventional plasmonic biosensing transducers. In the SPR transducer, p-polarized light is typically directed through a glass prism and reflected from a 50 nm Au film deposited on one of its facets. The SPR effect leads to a dip in the reflected intensity under an appropriate combination of angle of incidence θ and wavelength λ, whose value is resonantly dependent on the RI of a thin ($\sim$200 nm) layer near gold.[10] In alternative layouts, surface plasmon polaritons can be excited using metal grating couplers[12] or nano-hole arrays.[30] LPR transducers normally imply the excitation of uncoupled localized plasmons over Au or Ag nanoparticles or nanoparticle arrays, which leads to a resonant drop of intensity in transmitted or reflected spectra with its spectral position dependent on the RI of the environment around the nanoparticles (within the probe depth of 20–40 nm).[15,17]

Recent advances in the development of nanotechnologies have led to the appearance of novel optical biosensing transducers based on metamaterials. Plasmonic metamaterials for biosensing were introduced as artificial materials, composed of nanoscale plasmonic/dielectric blocks (meta-atoms) arranged in an array/lattice, which can outperform natural materials in terms of sensitivity to RI variations and enable new sensing functionalities.[31] Multi-layer structures, including multi-layer metal/dielectric stacks and 2D-plasmonic heterostructures, can also be classified as artificial materials (metamaterials). Examples of such metamaterial-based transducers include plasmonic nanorod metamaterials,[31] metamaterials based on coupled nanoparticle arrays,[32,33] heterometasurfaces combining 2D materials and plasmon-supporting metal films,[34,35] 3D metamaterials,[36] hyperbolic metamaterials based on multilayer stacks,[37] and Fourier metamaterials.[38]

In optical biosensing, several parameters could be used to detect biointeractions. Indeed, monochromatic light can be described by its amplitude, phase and polarization.[39] Both amplitude and phase can be employed as sensing parameters to follow bio-molecular binding events associated with the increase of the biofilm thickness. Due to the simplicity of acquisition, amplitude parameters (spectral or angular intensity) have been more widely used in SPR and LPR transducers. Optical phase is so far much less exploited as a sensing parameter, but can offer a breakthrough in sensitivity.

To start with, we will consider the parameters used to characterize the sensitivity of optical transducers and give a brief comparative analysis of detection limits of various transducers and parameters of interrogation (amplitude and phase). The sensitivity of a plasmonic transducer can be characterized in terms of the response of its sensing parameter to a unit variation of refractive index Δn of the environment (here, one assumes that RI of the whole bulk medium contacting the metal is changed). In particular, the spectral sensitivity in the case of SPR can reach 1000–4000 nm of wavelength shift per refractive index unit (RIU) change,[14] while in the case of LPR[15] and nanohole arrays[30] the relevant sensitivity is typically lower and does not exceed 200–400 nm RIU^{-1}. It should be noted that, in conditions of limited dynamic range of signal variations, the performance of plasmonic sensors is strongly affected by the width of resonances as the position of a narrow feature can be more precisely resolved by an instrumental system compared to a broader one. Such a resolution ability factor is taken into account in another parameter termed Figure-of-Merit (FOM), which describes the ratio of sensitivity to the width of resonances. In terms of FOM, SPR transducers demonstrate slightly better characteristics compared to LPR (20–25[14] and 8–10,[15] respectively), while the FOM of metamaterial nano-transducers can be improved up to values of 200 and higher.[40–43] This improvement comes from the excitation of diffraction-coupled surface lattice modes providing ultra-narrow (down to 2 nm FWHM) resonances.[40]

However, in practical biosensing measurements one is typically more interested in the limit of detection (LOD), which is the minimal detectable value of the monitored parameter. LOD depends not only on the sensitivity of the transducer, but also on the level of noise in the instrumental setup, which makes the choice of optimal interrogation parameter (and the related low-noise experimental arrangement for its recording) critically important. The optical LOD of plasmonic transducers can be described in terms of the minimal variation of RI that they can resolve. As an example, the optical LOD of SPR is estimated as $\Delta n \sim 10^{-5}$ RIU and can be further reduced to $\Delta n \sim (1\text{–}5) \times 10^{-6}$ RIU *via* feedback loops, signal filtering and processing methods,[14] while the use of less noisy

phase-sensitive schemes allows for orders of magnitude lower LOD. To describe the biosensing efficiency of plasmonic sensors, it is customary to use another parameter referred to as chemical LOD, which is typically described in terms of the minimal detectable concentration of a target analyte. It is clear that the chemical LOD depends on both the optical LOD and the efficiency of the biosensing recognition element. Due to planar geometry, the detection limit of a plasmonic biosensor can be also described in terms of the mass of biomaterial accumulating at the biosensor surface. Such LODs for conventional gold-based SPR and LPR platforms can reach values as low as 1 pg mm^{-2} [14] and 1 ng mm^{-2},[15] respectively, corresponding to $\sim$1 pg mL^{-1} and 1 ng mL^{-1} for common biomedical applications.

Fig. 2 summarizes the performance of optical transducers in amplitude and phase interrogations as reported in the literature. The *y*-axis of the graph shows the molecule size of the detected analytes in Daltons (1 Da is equal to 1 atomic mass constant or 1.6×10^{-24} g), while the *x*-axis shows the limit of detection (LOD) expressed in terms of the mass concentration g mL^{-1}. (LOD can also be expressed in molar units $M = 1$ mol L^{-1} with the help of the conversion LOD (g L^{-1}) = LOD(M)·molecule weight (Da)). Fig. 2 provides one of the main messages of this review: there exist particular transducers based on metamaterials and detection methods (phase interrogation) which, when compared to conventional SPR and LPR transducers, can provide a drastic improvement of both LOD and the ability to detect small molecules. The recorded parameters for these phase-sensitive metamaterial transducers are shown in green in the bottom-left corner of the graph.

In the next sections, we will discuss the origin of this extremely high improvement of the limit of detection for dedicated metamaterials[38] and present various metamaterial and device architectures enabling such hypersensitivity.

3. Going "beyond the limits" with enhanced phase sensitivity of "dark" architectures

3.1 Amplitude and phase interrogations in optical biosensing

Being an electromagnetic wave, light consists of orthogonal electric and magnetic field components illustrated in Fig. 3a by the vertical and horizontal sinusoids, respectively, which oscillate in time and space. The electric field vector of such a wave can be expressed as $\vec{E} = \vec{E}_0 \cos(kx - \varphi)$, where $E = |\vec{E}_0|$ and φ are the amplitude and the absolute phase of light, respectively: the amplitude is connected to the magnitude of the field, whereas phase describes the position of the beginning of the oscillation cycle.[39] The amplitude and phase present two key parameters for light wave interrogation. It is easy to see that other interrogation parameters are nominally connected to them or their derivatives: the polarization interrogations imply the measurements of light intensity $I = |\vec{E}_0|^2$ (an amplitude parameter) for two different polarizations or phase difference between them (a phase parameter), the wavelength interrogation is based on measurements of light intensities at different wavelengths, *etc.*

Let us consider a plane light wave that illuminates a selective biosensor transducer at some angle of incidence, Fig. 3b (a particular realization of the transducer is not important and a functionalized nanoparticle array is shown as an example). This light interacts with the transducer acquiring information

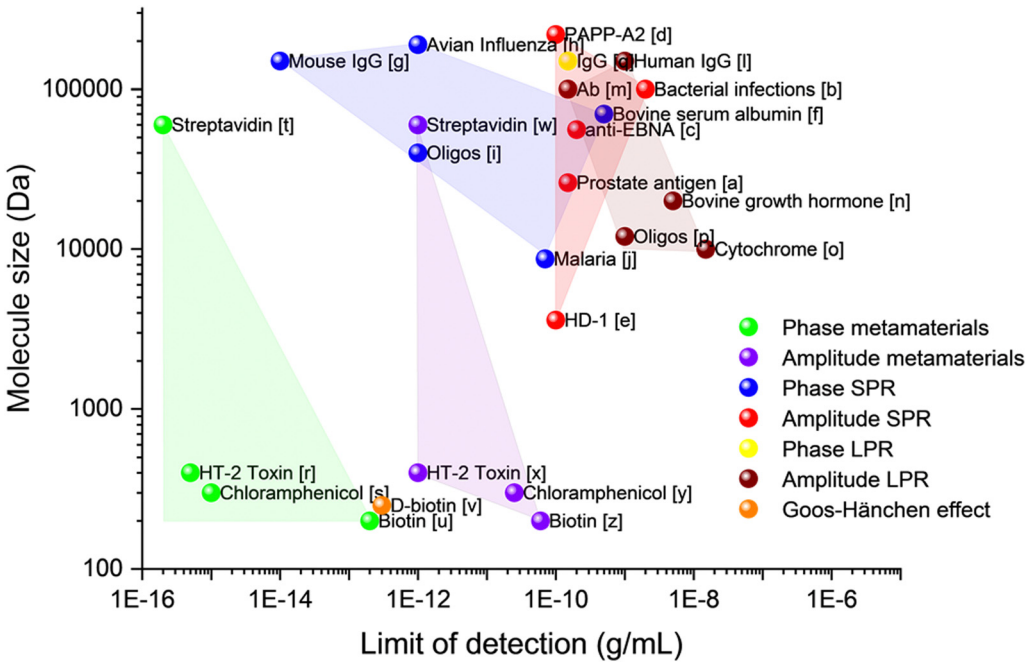

Fig. 2 Limit of detection for different plasmonic detection techniques. Data taken: [a],[44] [b],[45] [c],[46] [d],[47] [e],[48] [f],[49] [g],[50] [h],[51] [i],[52] [j],[53] [l],[54] [m],[55] [n],[56] [o],[57] [p],[58] [q],[59] [r],[60] [s],[38] [t],[33] [u],[61] [v],[62] [w],[33] [x],[60] [y],[38] [z].[61]

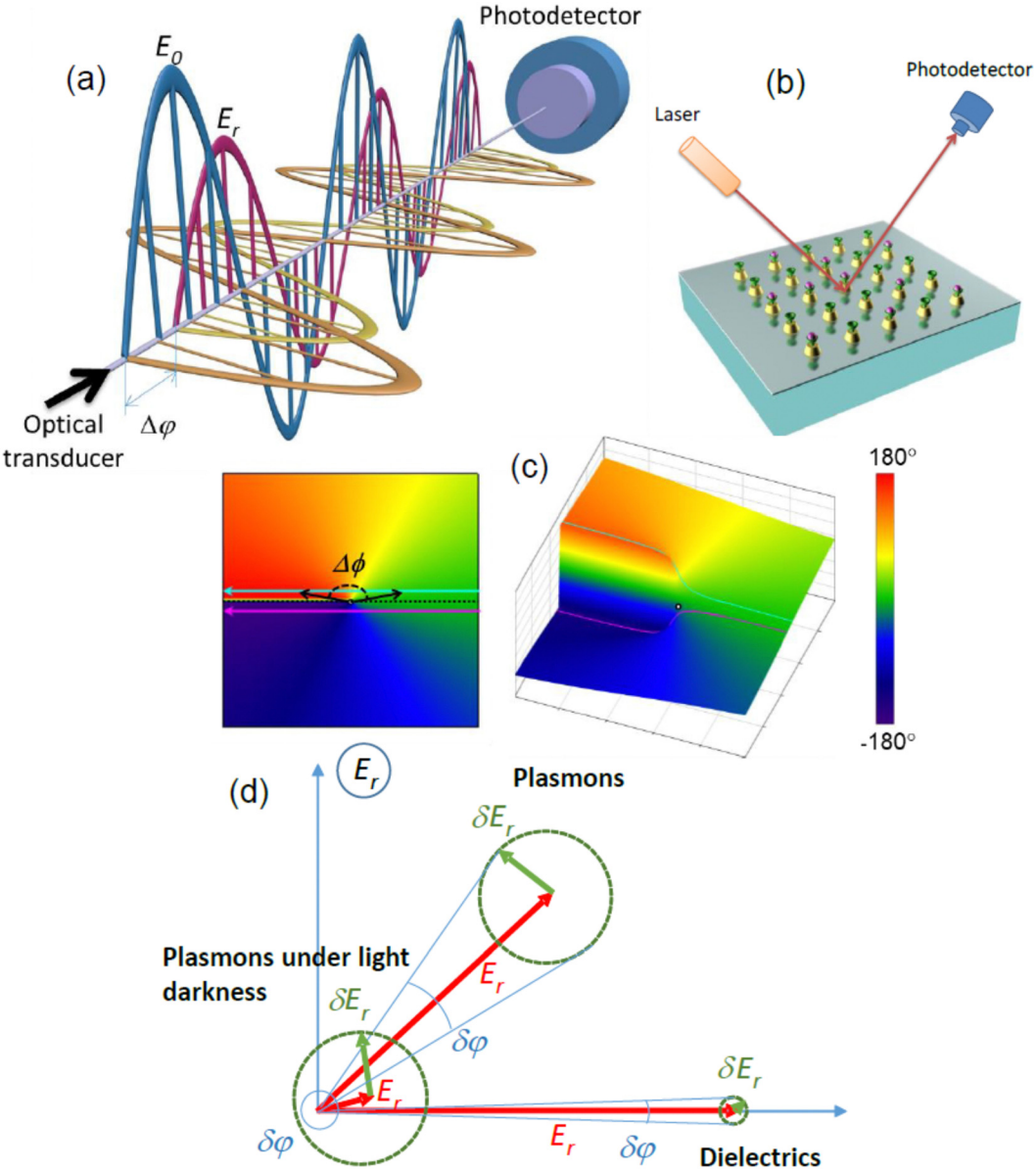

Fig. 3 Properties of light amplitude and phase. (a) Schematic of interference of two electromagnetic waves on a photodetector. Purple and golden sinusoids show amplitudes of electric and magnetic fields of a signal wave reflected from an optical biosensor transducer, while blue and orange sinusoids indicate relevant amplitudes for a reference plane wave reflected from a back mirror. Difference of phases of signal and reference waves $\Delta\varphi$ can be measured at any point through the common optical path and remains constant; (b) schematic of biosensing experiment. Light beam is directed onto an optical biosensor transducer (of any type), which can sensitively monitor variations of refractive index associated with binding events between a receptor (green caps) immobilized on the transducer surface and its selective partner from a solution (purple spheres), while optical information can be extracted in the reflected beam; (c) phase as a polar angle ϕ in the complex polarization plane E (left) and a 3D representation of the phase (right). It is visible that when the reflection from the sample approaches zero, shown by black arrows ($|E| = 0$ – the point of darkness represented by the white dot), a sharp phase singularity appears (blue and purple curves). The dotted black line corresponds to the Heaviside-like phase jump. The color map represents phase values at different points. Adapted from ref. 33 with permission from Springer Nature, copyright 2013; (d) comparison of phase and amplitude sensitivities for dielectrics, normal plasmons and plasmons at light darkness.

on biological interaction under study and then transmits this information to a reflected beam which is encoded in amplitude and phase data. (The selectivity is achieved through the functionalization of the sensor surface with receptors shown by the green cups, which selectively interact with analytes shown by the purple spheres.) Since the amplitude sensing response is related to a change of magnitude of electric field vector, it can be decoded by measuring light intensity I on a detector (intensity interrogation) as a function of light wavelength λ or angle of incidence θ (spectral and angular interrogation, respectively). In contrast, the phase sensing response is related to a phase shift of the wave. Such a shift cannot be extracted from the reflected wave alone and requires an additional reference plane wave (for example, such a reference wave can

be formed by splitting the original wave and then reflecting it from a suitably placed mirror). If the signal and reference waves are combined, the difference in phases of signal and reference beams $\Delta\varphi$ can be measured at any point along the reflected beam sufficiently far from the sample (Fig. 3a). In a case of plane waves, the relative phase $\Delta\varphi$ and the amplitude E_r define the reflected electromagnetic wave completely as $E_{refl} = E_r\cos(kx - \omega t - \varphi - \Delta\varphi)$. It is customary to use the complex representation of plane electromagnetic waves as $E = \mathrm{Re}(E_0\exp[i(kx - \omega t - \varphi)])$ and $E_r = \mathrm{Re}(E_r\exp[i(kx - \omega t - \varphi - \Delta\varphi)])$. In this case, the amplitude and the relative phase of the reflected wave can be expressed as complex field $E = E_r e^{i\Delta\varphi}$ in the complex plane $E = E' + iE''$, where the real part E represents in-phase vibrations of the electric field reflected by the sample (changing as $\cos(kx - \omega t - \varphi)$), while the imaginary part E'' represents out-of-phase vibrations of the reflected electric field (changing as $\sin(kx - \omega t - \varphi)$).[39]

Fig. 3c depicts the relative phase of light reflected from an optical system in this complex plane E, where the relative phase corresponds to the polar angle. Being plotted as a function of incident angle (or light wavelength), the reflected electric field forms a family of curves in the complex plane E. For simplicity, we show examples of two such curves with straight lines (blue and purple, Fig. 3c, left panel), although the results obtained are general and valid for curves of an arbitrary shape.[23] When these curves approach the coordinate origin (which corresponds to the point of light darkness $|E| = 0$), the angle (or wavelength) dependence of the phase of reflected light experiences a dramatic change. It is easy to see that there exists a curve shown by the dotted black line (between the purple and blue curves with a monotonic decrease and increase of phase, respectively) that corresponds to a 180°-jump in phase.[23] Hence, we expect to have high phase sensitivity of biosensing at the points of darkness due to abrupt changes of light phase.

Fig. 3d explains this high phase sensitivity for points of darkness by comparing the amplitude and phase responses for three typical biosensing systems: ''dielectric'', ''plasmonic'' and ''plasmonic structures at the point of light darkness''. As we mentioned above, when a selective reaction between bio-pairs takes place some number of analyte molecules will be trapped by the sensor, see Fig. 3b. As a result, the reflected field $\vec{E}_r$ would change by $\delta\vec{E}_r$ at the photodetector.[23] This leads to the maximal changes of reflected light intensity and phase as $\delta I_r \approx 2E_r\delta E_r$ and $\delta\varphi \approx \frac{\delta E_r}{E_r}$, respectively. (It is worth noting that maximal amplitude sensitivity is achieved at the condition when $\delta\vec{E}_r$ is parallel to $\vec{E}_r$ while the maximum of phase sensitivity is achieved when $\delta\vec{E}_r$ is perpendicular to $\vec{E}_r$.) Typical dielectric biosensing systems provide the in-phase optical response along the x-axis, see Fig. 3d, due to the nature of reflection from dielectric surfaces. Phase and amplitude sensitivities are modest for this case assuming that the reflection intensity is large. Plasmons provide enhanced electromagnetic fields on the surface of the sensor, which results in much larger δE_r and enhanced amplitude and phase sensitivity (see the plasmons response in Fig. 3d). The plasmons under light darkness, however, provide ultimately enhanced phase sensitivity. In this case, in addition to the enhanced response δE_r due to plasmon resonances, the reflected field amplitude is also made to be small ($E_r < \delta E_r$) such that the phase changes $\delta\varphi \approx \frac{\delta E_r}{E_r}$ are extremely large even for small δE_r, see the diagram for plasmons under light darkness on Fig. 3d. Such a phase response can improve the sensitivity of selective bio-reactions by 3–4 orders of magnitude when compared to the plasmon amplitude response. This consideration shows that the enhanced phase sensitivity will be observed for any point of darkness.

3.2 Darkness for phase detection and enhanced phase sensitivity in sensing

Optical darkness (essential for high phase sensitivity) can be created and utilised using several methods. Since optical reflection is produced by the interference of light emitted by secondary sources, there are two basic ways to achieve zero reflection. The first is to employ the radiation pattern of secondary sources and the second is to use interference.

3.2.1 Darkness through the radiation pattern. Normally, the secondary sources are small dipoles excited by incident light. A dipole cannot radiate waves in the direction of the induced dipole moment. This leads to the absence of reflection for p-polarized light that falls on an interface with refractive index n from the air at the so-called Brewster angle $\theta_B = \arctan(n)$. (There exist a handful of materials where secondary sources could be electric quadrupoles or magnetic dipoles,[63] which have different radiation patterns and therefore result in a different expression for the Brewster angle.).

The absence of reflection for p-polarization at the Brewster angle implies high phase sensitivity (see above) which is heavily used in ellipsometry.[64] At the same time, the darkness observed at the Brewster angle allows one to improve microscopy by realizing so-called Brewster angle microscopy[65] where a dark-field mode of a microscope is realized not through complex optics but through the Brewster phenomenon.

3.2.2 Darkness through interference. The most common way to achieve darkness is to use light interference. Examples include antireflection and dielectric coatings in which multiple beam interference is produced by light reflection from layered dielectric structures,[39] interference of scattered laser light which can be used to create optical vortex knots,[66] SPR in the Turbadar–Kretschmann–Raether configuration,[67] and hetero-metasurfaces based on graphene-protected gold and silver rendering possible almost zero reflectance.[34] Recent progress in nanofabrication has enabled the production of artificial metal-dielectric materials (also known as metamaterials and metasurfaces), which could be engineered to have the desired refractive index. With the help of light interference in a nanostructured thin film a plasmonic blackbody[68] (also known under the name of an ultra-thin perfect absorber[69]) was realized and the concept of topological darkness has been introduced.[33,36]

This concept allows one to generate darkness in a large variety of plasmonic systems (including 2D and 3D structures) important for biosensing.[33] Plasmonic surface lattice resonances observed in nano-arrays are another important phenomenon which allow one to achieve darkness in reflection, attenuated total reflection and even in light transmission which can be used to achieve extremely high phase sensitivity to detect bio-objects.[40] Singular nano-optics, topological phase singularities and light darkness were discussed for thin heterostructures by several groups.[70–72] It is worth stressing that plasmonic nanostructures with darkness are the best for achieving the tasks of biosensing: they provide unrivaled phase sensitivity combined with high (subwavelength) localization of the electromagnetic field and large field enhancement ratios, both important for single molecule detection.

3.2.3 Darkness renaissance. Recently, new ingenious ways to achieve darkness (relevant to biosensing) were implemented. Berkhout and Koenderink combined the concepts of radiation pattern and light interference to produce perfect absorption and phase singularities in plasmon antenna arrays etalons.[73] Thomas *et al.*[71] suggested employing strong light-matter coupling to realize all-optical control of darkness and phase. Topological darkness was realized even in extremely thin 2D atomic layers under appropriate conditions[74] and was shown to be useful for the tasks of biosensing. In a separate development, tunable darkness was demonstrated for exceptional point.[72] This darkness relies on the gain in the system. At the same time, new optical architectures to detect the phase of the light under darkness have recently been developed.[75]

In next sections, we will discuss various detection schemes, which allow one to achieve extreme bio-sensitivity.

4. Phase-improved plasmonic biosensors based on conventional SPR and LPR transducers

4.1 Phase-enhanced surface plasmon resonance

The operation and applications of SPR transducers were described in ref. 12–14 Since the most radical advances in the improvement of SPR sensitivity in the last 10–15 years were associated with the use of light phase as the sensing parameter, we will limit our consideration by the overview of phase-sensitive SPR schemes and trends in their further development.

The existence of a jump of phase of p-polarized light reflected from a gold film under the Turbadar–Kretschmann–Raether prism geometry and its strong response to variations of RI of the environment compared to amplitude parameters was reported by Abeles using ellipsometry measurements in 1976.[76] However, the potential of the phase-sensitive SPR technique for real-time characterization of bio-interactions was assessed much later. Kabashin and Nikitin[25,26] obtained a sharp phase jump under SPR by optimizing the thickness of Au film and then recorded a huge phase sensitivity of $\Delta\varphi/\Delta n \sim 10^5$ deg of phase per RIU change in optical models simulating RI variations. Assuming a relatively moderate instrumental resolution for phase measurements of $\sim 2\pi \times 10^{-3}$ deg, they estimated that the optical LOD of the phase-sensitive approach can be of the order of 10^{-8} RIU, which is at least 2 orders of magnitude lower than conventional amplitude SPR. The optical LOD at the level of 10^{-8} RIU was later measured experimentally in many independent studies (see, *e.g.*, ref. 24, 77 and 78), while much higher phase sensitivity compared to amplitude parameters was confirmed in numerous works (for a review, see *e.g.*, ref. 29). In ref. 24, the amplitude and phase sensitivities were discussed in detail and it was suggested that phase-sensitive schemes can provide much lower LOD owing to three fundamental reasons: (i) stronger probing field at the point of phase monitoring. Fig. 4a illustrates the phase and amplitude transformations under SPR. As shown in the figure, the SPR effect leads to a dip in reflected intensity and a sharp phase jump. Here, the maximal step-like phase variation takes place in the very minimum of the SPR curve, while the maximal intensity change is at the resonance slopes. The electric field probing the molecules is maximal for the conditions of optimal photon/plasmon coupling, *i.e.* in the minimum of SPR curve, where only variations of phase take place. It is estimated that electric field magnitudes at these two relevant points differ by about one order of magnitude, which results in one order of magnitude stronger response of phase to variations of RI; (ii) much lower level of (phase) noises. Under sufficient level of stabilization of thermal noises, the main instrumental noise limiting the LOD is caused by drifts of light source.[24] The level of phase noises can be lower than $\Delta\varphi/\varphi \approx 10^{-6}$ for commonly used laser sources, while relative intensity noise is usually at the level of $\chi = \Delta I/I \approx 10^{-2}$, see ref. 24. Owing to a much lower level of noises, phase characteristics can potentially provide a much lower LOD, assuming that the amplitude noises are subtracted using appropriate measurement schemes (see, *e.g.*, ref. 24 and 79); (iii) availability of additional options for phase signal processing and filtering. Since monitoring the phase of light inherently implies a relative measurement with respect to a reference wave, it allows for signal mapping that can be used to filter noise. In principle, a similar option is possible with amplitude parameters *via* the introduction of a reference channel, but this requires a considerably more complicated system, increasing cost.

Most works in the field of phase-sensitive SPR were devoted to the implementation of optical schemes which could minimize the level of LOD and obtain additional functionalities, including imaging and multi-channel sensing options, wide dynamic range, miniaturized sensor designs, *etc.* The main developments in the field of phase-sensitive SPR technology are given in ref. 29 and 80–82.

Significant effort has been applied to develop efficient instrumental implementations to extract the ultrasensitive phase response. Polarimetry is the most straightforward phase detection approach based on the analysis of phase-polarization characteristics in a single beam containing p- and s-polarization components. Since only the p-component is affected by the SPR effect, the s-component is used as a reference. These components are brought into interference *via* the use of a polarizer, while phase variations in the p-polarized component are determined *via* a series of intensity measurements using appropriate

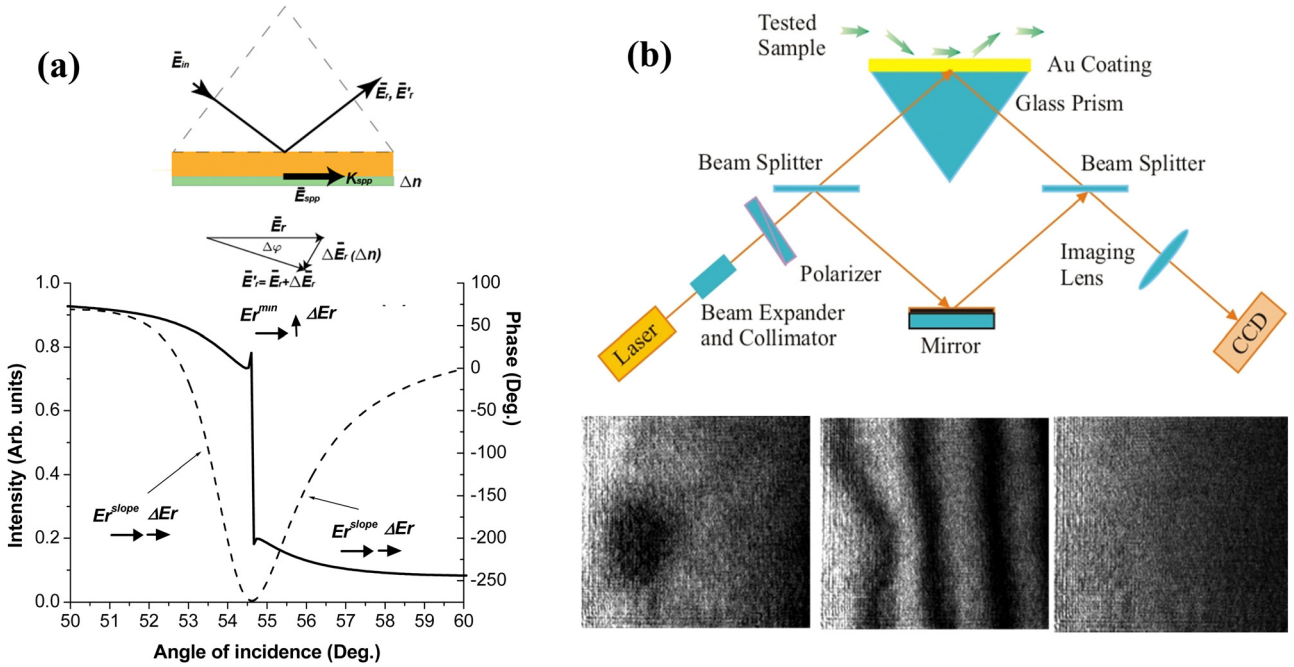

Fig. 4 Phase sensitivity under SPR. (a) Transformations of light electric vector under SPR (upper panel). Angle dependencies for reflectivity (dashed) and phase (solid) under the optimal thickness of the SPR-supporting gold. Adapted from ref. 24 with permission from Optica Publishing Group, copyright 2009; (b) schematic of SPR Mach–Zehnder interferometer and images of a thin droplet of a fatty acid of 1 mm in diameter on a gold surface obtained in Zernike phase contrast mode (lower left) and fringe mode of the interferometer (lower center), as well as in amplitude microscopy mode (lower right). The droplet is clearly resolvable in first two phase-sensitive modes, while conventional SPR microscopy is not capable of detecting it. Adapted from ref. 23 with permission from AIP Publishing, copyright 1999.

phase shift algorithms. Ellipsometry is the most elaborated and robust polarimetry technique, which provides the angular or spectral dependence of the ellipsometric reflection (Ψ) and phase shift (Δ), related to the ratio of the electric field amplitudes for p and s polarized components and the phase difference between them, respectively, such that $\tan(\Psi)\exp(i\Delta) = E_p/E_s$.[64] Ellipsometry serves as the main tool to characterize phase properties of sensing transducers, but this instrument is not well adapted for measurements of low LODs due to high noise levels. Alternative polarimetry systems can be implemented in simplified designs, *e.g.* ones using rotating analyzers[83] or spatial beam modulators,[84] and in more sophisticated schemes employing the temporal modulation of light phase by liquid crystals[85] or photoelastic (PEM)[79,86–88] modulators, *etc.* In time-modulation schemes, one can extract the phase response at different harmonics of the modulation frequency, and then use electronic processing methods for noise reduction to reduce the detection limit down to 10^{-8} RIU and lower. Polarimetry methods can be also applied to improve the contrast of signal patterns in angular[89,90] and spectral[91] interrogation schemes of conventional SPR, or to improve microscopy schemes.[92–94] Similar in many respects to time-modulated polarimetry, optical heterodyning records the differential frequency between two frequency-shifted orthogonally polarized s- and p-components of light reflected under SPR,[50,95] which also allows for efficient noise removal and the minimization of LODs down to 10^{-8} RIU. However, imaging prospects of this approach look complicated. The third phase-sensitive method is based on interferometry, in which signal and reference beams have fully or partially different optical paths, forming a steady interference pattern in the spatial domain. Presenting a more general approach compared to polarimetry and optical heterodyning, interferometry can offer simple optical extraction/visualization of phase information and a much easier implementation of imaging and multi-channel sensing schemes, although the treatment of optical image signal is typically more complicated in such schemes. SPR interferometry was first demonstrated in the Mach–Zehnder geometry[25,26] and then extended to a series of other implementations, including differential phase,[27] multi-pass Michelson,[96] and Fabry–Perot[97] interferometry. Interferometry is currently the most popular phase-sensitive SPR scheme, designed to either give access to ultra-low LODs or enable imaging functionality.

The development of spatially resolved imaging schemes for microscopic characterization and parallel sensing in multiple channels is one of the main trends in the development of phase-sensitive SPR technology. As shown in ref. 23, the resolution of phase-sensitive interferometric imaging is so high that it makes possible the visualization of organic objects which cannot be resolved with conventional amplitude-sensitive microscopy (Fig. 4b). In addition, this geometry can work with multi-channel structures with cell dimensions corresponding to gene chips and high throughput screening platforms ($100 \times 100\ \mu m^2$). A variety of designs based on both polarimetry[92,93] and interferometry[28,52,98] were later presented to enable phase-sensitive microscopy. Some of these schemes enable parallel

sensing in multiple channels (up to several tens) and applied for protein[28] and DNA[98] detection. Several studies were devoted to the minimization of image noise and the improvement of the resolution of microscopy images. As an example, Wong *et al.*[99] proposed a time-modulated interferometric scheme with the control of phase in every pixel of the image, in which interference patterns between p- and s components are separated, while the monitoring of differential phase allows one to minimize noise and thus improve the image resolution. As another example, Somekh *et al.*[100] proposed a wide-field design composed of a speckle-illuminated Linnik interferometer that could combine high lateral resolution of microscopy images and high detection sensitivity.

Another direction of research addresses the extension of the dynamic range of phase-sensitive measurements, which is limited due to a finite value of phase jump. Markowicz *et al.*[87,88] proposed a polarimetry scheme based on a photoelastic modulator, in which a signal recorded at the 2nd and 3rd harmonics of the modulation frequency presented a mixed response of phase and intensity, leading to a combination of relatively low LOD (2.9×10^{-7} RIU) and a wide dynamic range of measurements (10^{-2} RIU) due to phase and intensity contributions, respectively. Ng *et al.*[49] suggested a differential interferometry scheme based on the simultaneous analysis of the phase of p- and s-components of white light spectra, in which a proper selection of wavelength enables one to probe any refractive index value of interest and thus combine low LOD (2.9×10^{-7} RIU) and wide dynamic range (better than 10^{-2} RIU). Huang *et al.*[101] proposed the configuration of a SPR sensor with a phase retardation element based on a stacking liquid crystal modulator (LCM), which can also combine phase detection and angular interrogation in order to achieve a low LOD (2.2×10^{-7} RIU) and wide dynamic range. Using innovative designs based on differential interferometry between the focused radially polarized and azimuthally polarized (AP) cylindrical vector beams in a high numerical aperture (NA) objective-focusing geometry, Wang *et al.*[102] demonstrated wide dynamic range measurements in a phase-sensitive microscopic implementation.

The miniaturization and integration of the sensor transducer and other optical elements in compact designs is another important direction in the development of the phase-sensitive SPR technique, which promises the improvement of portability and cost-efficiency of this technology. Several phase-sensitive schemes using compact designs were proposed, including single mode SPR waveguides,[103] compact integrated SPR interferometers,[104] symmetric metal cladding waveguides,[105] waveguide-based Bragg grating structures[106] and SPR photonic crystal waveguides.[107] Patskovsky *et al.*[108,109] adopted the SPR technique for a silicon platform, which opened up novel opportunities for a radical miniaturization of the phase-sensitive SPR technique and its integration into standard Si-based processing technology. Another promising approach is related to the development of smartphone platforms based on the integration of lightweight optical components and sensing elements on a phone case,[110] which opens up access to portable sensor designs for biomedical, health and environmental monitoring applications.

The search of novel sensing formats and architectures is another important trend in the development of phase-sensitive SPR technology. One interesting sensor architecture uses nanohole arrays in thin gold films to excite surface plasmon polaritons.[30] Cao *et al.*[111] showed that light phase can have a very sharp phase jump under these conditions with the narrow linewidth of about 0.35 nm FWHM leading to a large phase FOM of almost 2000 RIU^{-1}, while the relevant spectral sensitivity (685 nm RIU^{-1}) is still 5 times lower compared to conventional prism-based SPR due to correlation of its value with the array periodicity.[30] In other works, Lee *et al.*[112] proposed a spatially-resolved microscopic design based on nanohole arrays and demonstrated full spectral imaging and simultaneous affinity monitoring from 50 microfluidic channels. Gold nanoparticle-based signal enhancement is another interesting technique for phase-sensitive SPR, although this technique does not have the benefits of label-free detection. Prasad *et al.*[113] explored the use of Au nanorods with different aspect ratio as labels for signal enhancement and showed that the maximal phase response takes place under the coupling between LPR over Au nanorods and SPR over the sensing film. The use of nanoparticle-based signal enhancement resulted in 23-times and 40-times lower LOD in the detection of trace-amounts of anti-rabbit IgG[113] and tumor necrosis factor alpha (TNF-α) antigen,[114] respectively. Zhou *et al.*[52] demonstrated that the nanoparticle-enhanced technology can be adapted for phase imaging to enable ultrasensitive biosensing of proteins and DNAs in oligonucleotide and aptamer microarrays. Zhao *et al.*[115] proposed a novel design of a phase-sensitive SPR sensor employing asymmetric Fano resonances, formed by the interaction of evanescent waves of the conventional surface plasmon polariton mode, generated at metal/dielectric interface, and a dark planar mode over multilayers consisting of dielectrics with alternating low and high refractive indices. By using the 3-point method to examine polarization information reflected from the transducer, the authors recorded a sharp signal change from the Fano resonance and at least one order of magnitude better LOD of the phase-sensitive signal compared to its amplitude counterpart, which was recorded in measurements of DNA hybridization. Exploring alternative materials for SPR excitation, Qui *et al.*[116] showed that 29.8 nm thick TiN films can reproduce the SPR effect and provide a LOD lower than 2×10^{-7} RIU in phase interrogation, while the TiN surface was expected to provide a better affinity to some biomolecules compared to Au.

As the benchmark of the success of phase-sensitive SPR, some designs of this technology were successfully commercialized (see, *e.g.* BiOptix 404pi unit, Bioptix Analytical Inc., **https://www.bioptixanalytical.com**) to offering improved sensitivity and multi-channel sensing.

4.2 Phase-enhanced localize plasmon resonance in arrays of randomly distributed nanoparticles

Localized plasmon resonance over substrate-supported nanoparticle arrays can offer several advantages over SPR. First, owing to the lack of translational symmetry, the excitation of

LPR does not require momentum matching and can be done in a simple transmission or reflection geometry using spectral interrogation to control the position of the plasmonic resonances. Second, in some cases LPRs can benefit from cost-efficient fabrication routes for metal nanoparticles and nanoparticle arrays (*e.g.*, by nanosphere lithography[15] or thermal annealing of thin Au films[117]). LPRs can offer a series of unique properties and functionalities, including spectral tuneability by varying the nanostructure size and shape, size selectivity, electric field enhancement to enable a SERS channel, *etc.*[15] LPRs have at least an order of magnitude lower sensitivity to bulk refractive index variations compared to SPR, but in some biosensing tasks this sensitivity handicap is compensated by a higher localization of probing electric field (30 nm compared to 200 nm).[15] Indeed, the resonant shift upon molecular adsorption can be similar for LPR and SPR due to a better overlap between the probing field and the size of relatively small target molecules in the case of LPR.[15]

Randomly distributed nanoparticles illuminated by light scatter the light independently, with random phase relations between scattered rays. Therefore, LPRs are broad, typically having a FOM lower than four,[15] which limits the resulting LOD. Considering the excitation of LPRs in randomly distributed gold nanodisks and nanorings on top of a continuous gold layer and a dielectric spacer, Lodewiijks *et al.*[118] demonstrated that the FOM can be boosted by almost an order of magnitude by extracting information on the phase of light and its proper mathematical treatment. This result was explained by the much narrower spectral linewidth of the phase jump, which is located only near the very minimum of the LPR curve. In another study, Piliarik *et al.*[58] showed that the technique of phase-polarization contrast, originally developed for the enhancement of signal images under SPR,[89–91] can be extended to the LPR sensing geometry and applied in imaging layouts.

The use of phase sensitivity under LPR opens up additional advantages. Using ellipsometric technique, Moirangthem *et al.*[117,119] studied the phase response in the ATR geometry from glass-supported and partially embedded 50–80 nm gold nanoparticles produced by thermal annealing of Au films and the deposition of colloidal nanoparticles. Depending on the original size of nanoparticles, they recorded positive and negative resonant features in the reflected ellipsometric parameter Ψ, accompanied by abrupt phase jumps in the resonances, which were attributed to different plasmon modes. The authors recorded bulk phase sensitivity of 2×10^3 deg RIU^{-1} for nanoparticle arrays produced by thermal annealing of Au films (for colloidal nanoparticles, the sensitivity was 2.5-fold lower), and reported a LOD of 20 pM in the interaction between mouse anti-EGFR and goat anti-mouse IgG (secondary antibody). Using a cost-efficient hole-mask colloidal lithography, Svedendahl *et al.*[120] fabricated random arrays of nanodisks of particular size characteristics (Fig. 5a), which provided Fano-type asymmetric resonances due to the interaction between LPRs from the nanoparticles and a broad reflection from the substrate/water interface, yielding a nearly zero reflection under the illumination by s-polarized light in the ATR geometry (Fig. 5b). Although the bulk spectral sensitivity of these arrays was low (178 nm RIU^{-1}) and their resonances were relatively broad, the relevant phase sensitivity reached 1.5×10^4 deg RIU^{-1} due to the presence of an abrupt phase jump in the minimum of such Fano resonances,[120] in accordance with the previously stated concept of topological darkness.[23,33] The applicability of the proposed sensor architecture was confirmed in the model reaction using NeutrAvidin-biotin affinity, while phase sensitivity was at least one order of magnitude better than the spectral one. Fig. 5c shows the experimental phase difference between p- and s-polarized light with the Heaviside-like π-jump observed at the incident angle of 55° (Fig. 5c) and extremely high raw phase sensitivity to small changes of refractive index of water–glycerol mixtures (Fig. 5d).

Wu *et al.*[59,121] demonstrated a technique of spectral differential interferometry for low-noise control of LPRs excited in self-assembled metal nano-islands formed by thermal annealing of thin films and adapted for biosensing. They confirmed that an extremely sensitive phase response can be observed even in an unordered array of gold nanoparticles and claimed that the functionalization of dielectric glass substrates in ''hot spots'' between the gold nano-islands can provide additional signal amplification due to local electric field enhancement.[59] The group also demonstrated successful applications of LPRs in the nano-island geometry in biomedical tasks, including the detection of tumor-derived extracellular vesicles at levels lower than 0.194 μg mL^{-1}.[122]

5. Ultra-sensitive biosensing with hetero-metasurface-based transducers

Heterostructures can be easily incorporated into the SPR geometry of surface plasmon excitations. Their usage allows one to (i) improve the quality and darkness of SPR, (ii) achieve SPR spectral tuneability and (iii) combine plasmonic modes with waveguide modes of heterostructures. Hence, it was not surprising that bimetallic Au/Ag or Au/Cu films were used to increase the resonance quality of SPR, while an additional thin oxide layer was employed to adjust the resonant wavelength and increase the amplitude sensitivity.[12] After the isolation of graphene and a whole family of 2D materials,[123] 2D material heterostructures became a prominent subject of study in SPR biosensing. 2D atomic materials have an extremely small thickness (which could be just one layer of atoms) and combined with SPR excitation they yielded several new functionalities: (i) the possibility to protect reactive metals with excellent plasmonic characteristics, whose usage for SPR detection is restricted by metal oxidation,[34] (ii) an increased surface area of some 2D coatings (*e.g.*, graphene oxide or reduced graphene oxide), which can result in higher biosensitivity,[124] (iii) new bio-functionalization procedures based on 2D material functionalization which are refreshingly different from those based on gold.[60] (It is worth mentioning that 2D materials can also provide tuneability of resonances and their coupling with

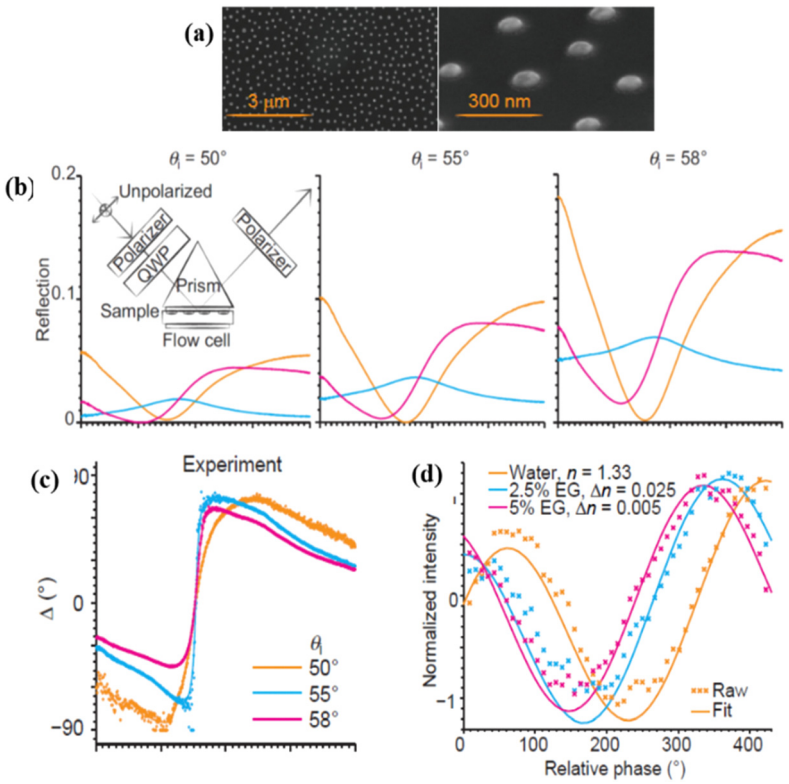

Fig. 5 Phase sensitivity in arrays of random plasmonic nanoparticles. (a) SEM images of gold nanodisk arrays deposited on a glass substrate. The nanodisks had 86 nm diameter and 20 nm height; (b) experimentally measured reflection for light of three different polarization states: R_s (orange), R_p (blue) and R_{s+p} (pink) from a sample illuminated by circularly polarized light. The latter state is an equal mix of s- and p-polarized reflection components. The three panels show reflections for three different angles of sample illumination (θ_i = 50°, 55°, 58°). Experimental setup is shown in the inset; (c) experimentally measured phase difference between p- and s-polarized light; (d) bulk refractive index sensing with a single wavelength phase detection scheme. The fringes shifted when pure water was replaced by different concentrations of ethylene glycol solution, as shown in the panel. Adapted from ref. 120 with permission from Springer Nature, copyright 2014.

waveguide modes, as well as to sustain intrinsic plasmons[125] that can be used for efficient biosensing.[126]) Heterostructures and 2D materials were widely used in conventional amplitude SPR devoted to human health applications. For example, 0.5 M lysozyme was detected on aptamer-functionalized reduced graphene oxide-coated SPR chips,[127] a graphene/MoS_2/waveguide layer heterostructure was shown to provide a three orders of magnitude increase of sensitivity over gold SPR,[128] Ni doped graphene was used to improve the sensitivity of LPRs to 3-nitro-L-tyrosine (a biomarker of neurodegenerative diseases) to the level of 0.13 pg mL^{-1},[129] Au-graphene-oxide-COOH chips were used to detect cytokeratin 19 biomarker (connected to lung cancer) with a LOD 0.05 pg mL^{-1}.[130] Some of these advances were recently reviewed in ref. 18.

In this section, we review applications of heterostructures and 2D materials for phase sensitive plasmonic detection. A lot of progress has been made both in theory and experiments and we start with experimental works. The most obvious application of 2D materials in biosensing comes from the fact that 2D materials are extremely thin, impenetrable to oxygen and water and mechanically tough. As a result, 2D materials were immediately used to protect the plasmonic properties of reactive metals, such as copper, silver and others with the aim of realizing SPR resonances that would be better than those based on the conventional gold architecture. Kravets *et al.*[34] developed techniques that allow one to protect copper and silver SPR films using graphene monolayers, which yielded plasmon resonances of better quality than those of conventional gold. This work made possible plasmonic resonances based on copper films with extremely high phase sensitivity, demonstrated using graphene hydrogenation that showed 0.2 fg mm^{-2} surface sensitivity of a graphene protected copper SPR sensor.[34] It is worth stressing that this is four orders of magnitude better than the amplitude sensitivity of analogous gold SPR chips. The amplitude sensitivity of graphene protected copper SPR chips of 5600 nm RIU^{-1} was also better than that of gold films in the same spectral range.[34] 2D materials can offer refreshingly different functionalization techniques (as compared to gold), enabling selective biosensing. As a result, Wu *et al.* introduced a layered material platform for ultrasensitive phase biosensing[60] based on the technique of protecting plasmon-supporting metal films with various 2D materials (graphene, hBN, *etc.*) combined with developed protocols of 2D material functionalization. Using this platform, HT-2 toxin (~424 Da) was detected in PBS solution and beer by copper SPR chips protected by functionalized graphene with the amplitude detection limit of ~1 pg mL^{-1} and the phase

sensitivity limit of ~0.5 fg mL^{-1}, which is comparable with best results obtained with labelling techniques,[60] see Fig. 2.

Fig. 6a and b display the changes of amplitude and phase of light for PBS solution containing ~1 pg mL^{-1} HT-2 toxin. The largest phase sensitivity occurred at the wavelength λ = 747.40 nm that corresponded to the darkest resonance where a phase jump of $\delta\Delta > 100$ degrees was observed with no substantial change in the light amplitude. Fig. 6c and d show spectral resonance dependences after pumping different concentrations of HT-2 toxin in PBS through the SPR cell. The resonance position followed the Hills law as shown in Fig. 6(e) and (f). Using graphene protected copper SPR chips and different functionalization procedures, short DNA segments corresponding to malaria were recently detected with high accuracy[53] which could open way to inexpensive in-field detection of malaria. Following this research, composite metal-dielectric-graphene hybrid heterostructures were fabricated with plasmon resonances sensitivity of 30 000 nm RIU^{-1}.[131]

Graphene and graphene oxide can also be used to improve the phase sensitivity of conventional gold SPR chips. This was done in the work Zeng *et al.*[35] where the combination of graphene and a conventional gold film was used to achieve a high sensitivity. Using a protocol of single-stranded DNA (ssDNA) on a graphene/gold metasurface, the authors reported the phase sensitivity of 1×10^{-18} M, which is claimed to be 3 orders of magnitude higher than any state-of-the-art plasmonic sensors. The selectivity of the detection came from the ability of the graphene-based substrate to selectively attach some molecules through pi-stacking forces. The proposed geometry provides a simple and robust way to selectively detect aromatic rings in bio-objects such as DNA, RNA, peptides and cytokines. Instead of graphene, Wang *et al.* covered gold films with atomically thin $Ge_2Sb_2Te_5$ to achieve a zero reflection phase singularity in the attenuated total reflection configuration and giant phase sensitivity of TNF-α cancer biomarkers.[132] The detection limit of phase interrogation was experimentally demonstrated to be 10^{-15} mol L^{-1}. These results hold promising potential in biomedical applications and clinical diagnostics.

Surface plasmons used in biosensing can be also excited by periodic gratings. When deposited on the surface of a metal

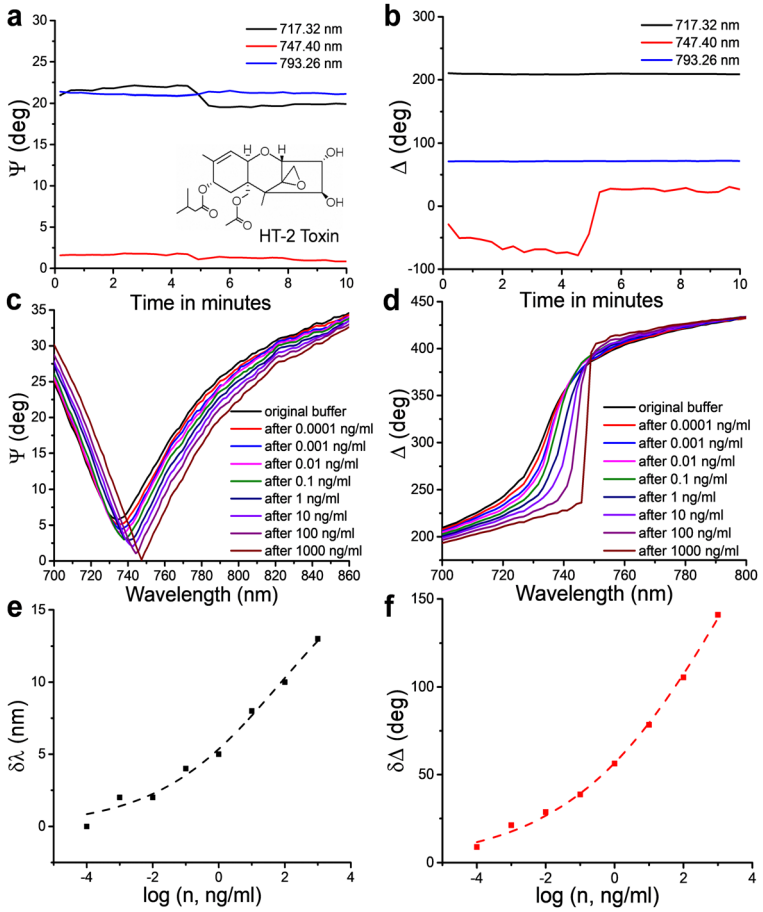

Fig. 6 Phase SPR biosensing of HT-2. (a and b) Ellipsometric parameters ψ (amplitude) and Δ (phase) of the SPR curve of functionalized GPC chips at 717.32, 747.40 and 793.26 nm, as a function of time when the sensor chip reacts with HT-2. The pumping time of PBS is ~4.5 min. The inset in a shows the molecular structure of HT-2. (c and d) SPR spectral curves after reacting with different concentrations of HT-2 in PBS. (e and f) The shift of resonant wavelength ($\delta\lambda$) for ψ and the change of phase ($\delta\Delta$) as a function of logarithm of concentration, n, of HT-2. The dark dashed line shows the sigmoidal fits (Hill's law) of $\delta\lambda$ as a function of log(n), and the red dashed line is the same for $\delta\Delta$, giving n_H = 0.2 ± 0.01 and $K_H > 1$ μg mL^{-1}. Adapted from ref. 60 with permission from Springer Nature, copyright 2019.

film, these gratings form nanostructured heterostructures and can efficiently couple light to surface plasmon polaritons. Using this geometry (which is particularly suitable for lab-on-a-chip architectures), Rossi *et al.*[133] performed phase sensitive detection of a standard biotin–avidin reaction. The careful optimization of experimental parameters led to a 30–50% enhancement of sensing response, opening new possibilities for applications in biomedical research while maintaining the ease and versatility of this configuration. Another way to achieve high phase sensitivity using optical metasurfaces was demonstrated in ref. 134 where designer metasurfaces were used to produce light interference patterns which were dependent on the phase response of just a single nanoantenna. Such metasurfaces could improve the phase response of plasmonic biosensors.

Theoretical work has concentrated on various possible geometries combining plasmonic metal (or a sandwich made of two different metals) with graphene, hBN and layers of various transition metal dichalcogenides (TMDCs) such as MoS_2, WS_2, *etc.* Following the ideas of protecting and enhancing metal SPR with graphene,[34] Zeng *et al.*[128] theoretically discussed the properties of gold SPR chips covered by two different 2D materials: MoS_2 and graphene. The proposed metasurface system promised a phase-sensitivity enhancement factor of more than 500 when compared to the SPR sensing scheme without the graphene–MoS_2 coating or with only a graphene coating. The authors attributed this improvement to a higher optical absorption efficiency of the MoS_2 layer. An analogous structure with an added ZnO sublayer (below the gold film) was discussed in ref. 135. The optimized hybrid structure of zinc oxide (40 nm)/gold (42 nm)/monolayer MoS_2/graphene was found to result in dark SPR with extremely high phase sensitivity.

Noble metal/TMDC based heterostructures precisely engineered to achieve significant phase sensitivity improvement were discussed in ref. 136. The theoretical analysis showed that they result in low values of minimum reflectivity R_{min} (at the level of $\sim 10^{-8}$) for excitation wavelength of 1024 nm calculated for Au/Si/WS_2 and Au/Si/$MoSe_2$ sandwiches. The dark singularity at the resonance dip led to a high phase sensitivity of 10^7 deg RIU^{-1}, which is three orders of magnitude higher than that with bare metallic sensing substrates used in commercial plasmonic sensors. Han *et al.* utilized various TMDCs (WS_2, MoS_2, WSe_2, $MoSe_2$) in a complex Ag-ITO-TMDCs-graphene heterostructure.[137] The highest phase sensitivity of 3.6×10^6 deg RIU^{-1} was obtained using 3-layered MoS_2 and 4-layered graphene. Analogous results were obtained in a recent theoretical work.[138]

Even more complicated heterostructures for phase biosensing were theoretically discussed in ref. 139. The authors proposed a TMDs/metal/TMDs/graphene heterostructure and claimed to calculate extremely high phase sensitivity of $\sim 10^5$ deg RIU^{-1} for aluminum metal films sandwiched by MoS_2, $MoSe_2$, WS_2 and WSe_2 layers. Other theoretical works include the study of a nanohole array for phase sensitive biosensing,[140] an application of 1D photonic crystals covered by graphene for phase detection,[141] a study of the phase response of a bimetallic Au/Ag SPR heterostructure protected by graphene,[142] an application of Fano resonances in 2D heterostructures for high phase sensitivity[143] (phase sensitivity up to 10^6 deg RIU^{-1} was achieved), the use of a hBN planar waveguide in Fano resonances for phase response,[144] a study of phase-sensitive SPR sensors based on Metal–ITO-TMDC hybrid multilayers.[145] Complex multilayers capable of supporting Tamm states have been suggested for optical detection.[146]

6. Ultra-sensitive biosensing with coupled nanostructured plasmonic metamaterials

6.1 Generation of extreme phase singularities in plasmonic metamaterials

As explained above, the behavior of the phase of light becomes singular and experiences fast changes at the conditions of light darkness (as phase is undefined for the zero value of light intensity). Thus, the highest phase sensitivity of biosensing transducers is expected from plasmonic systems that realize close to zero light reflection. SPR and LPR transducers present simple geometries of plasmon excitation, which provide higher sensitivity in their phase response than in their amplitude response, but light intensity cannot approach zero under these geometries due to particular plasmon coupling conditions. As we showed in the previous chapter, the limitation can be overcome by the employment of heterometasurface transducers. Another radical way to solve the problem consists in the use of cleverly designed metamaterials, composed of nanoscale blocks arranged in a lattice, which enables their ''shaped'' optical response due to the coupling of plasmonic elements in the structure (electromagnetic coupling,[147,148] plasmonic coupling,[149] resistive coupling,[150] *etc.*). By carefully designing nanostructured or nano-heterostructured plasmonic systems, one can tune the optical response to provide near-zero light reflection (or transmission) and thus generate singularities of light phase, opening up access to virtually unlimited phase sensitivity.

Conditions for the implementation of light darkness in such plasmonic systems were examined by Kravets *et al.*[33] In their model, a layer of bio-functionalized plasmonic material (it could be a flat or nanostructured layer) was described by effective optical constants n and k, which gave the complex refractive index of the layer by $N = n + ik$. It was shown that for a fixed angle of incidence and a fixed (small) thickness of the layer, there exists a curve of exactly zero reflection provided by Fresnel coefficients (in the case of the absence of scattering). They also demonstrated that thin metallic layers can not provide zero reflection due to particular optical constants of metals. On the other hand, properly designed nanostructured metamaterials can yield optical constants that cross the zero reflection curve and the corresponding reflection from the nanostructure can have a well-defined point of complete darkness.[36]

Subsequent studies have shown that similar effects can be obtained using a range of phenomena in nanostructured metamaterials. Below, we will present these metamaterials, which open access to extreme sensitivity, promising a breakthrough in the improvement of detection limit for a plethora of biosensing applications.

6.2 Hyperbolic (meta)materials enabling extremely high sensitivity

Hyperbolic metamaterials (HMMs) present a promising platform for the implementation of ultra-high sensitivity. These artificial nanostructured metamaterials can profit from specific hyperbolic optical dispersion, which relates the wavelength λ (or wavenumber k) of a wave in a medium to its frequency ω. In contrast to the elliptical dispersion of normal homogenous isotropic materials described by $k_x^2 + k_y^2 + k_z^2 = \omega^2/c^2$, hyperbolic dispersion implies the presence of a strong uniaxial material anisotropy leading to a particular dispersion relation: $(k_x^2 + k_y^2)/\varepsilon_{zz} + k_z^2/\varepsilon_{xx} = \omega^2/c^2$, where dielectric constant presents the tensor $\bar{\varepsilon} = [\varepsilon_{xx}, \varepsilon_{yy}, \varepsilon_{zz}]$. In hyperbolic metamaterials, the out-of-plane dielectric component $\varepsilon_\perp = \varepsilon_{zz}$ has the opposite sign to $\varepsilon_\parallel = \varepsilon_{xx} = \varepsilon_{yy}$.[153] Here, one can imagine two opportunities related to negative and positive values of ε_{zz}, which correspond to "Type I" and "Type II" hyperbolic metamaterials, respectively. Type I metamaterials can be realized in the case of an assembly of densely packed long (300–500 nm) metal nanorods, oriented perpendicular to a glass substrate (Fig. 7a). The illumination of such arrays in ATR geometry leads to the excitation of a guided mode G over the nanorod assembly, which provides a much higher spectral sensitivity to RI variations (32 000 nm RIU^{-1}) compared to SPR and LPR counterparts and a high FOM exceeding 330.[31] As shown by Sreekanth *et al.*,[37] Type II hyperbolic metamaterials can be realized under the arrangement of a stack of metal/dielectric bilayers (Fig. 7b), which enables the excitation of plasmon waves coupled evanescently in adjacent bilayers, yielding highly confined modes ranging from visible to infrared wavelengths. By exciting these modes using a grating coupler, the authors reported a similar sensitivity level of 30 000 nm RIU^{-1} and even higher FOM (up to 590) of some resonant modes.

Both types of hyperbolic metamaterial demonstrate excellent prospects for phase-sensitive plasmonic biosensing due to their deep, high-quality resonances and a high electric field concentration in the probed region. In particular, using a prism coupler, Sreekanth *et al.*[62] excited hyperbolic modes in a HMM based on a multi-layer Sb_2S_3–TiN geometry (Fig. 7c), which was expected to have lower losses compared to noble metal-based HMMs. As shown in Fig. 7d and e, the excitation of such modes is accompanied by deep resonance dips in the angular dependence of reflected intensity and very abrupt jumps in differential phase between TM and TE polarization components, whose properties could be tuned by using the amorphous or crystalline phase of Sb_2S_3 (black and red curves, respectively). The phase sensitivity of this HMM, determined by using a range of glycerol/water mixtures, was about 8×10^3 deg RIU^{-1}, which is very promising for biosensing applications. By depositing a graphene layer on the HMM element, the authors also designed a prototype apto-biosensor and reported real-time binding of thrombin at concentration of 10^{-15} M.[152] In a separate study, Wu *et al.*[155] proposed an alternative design of

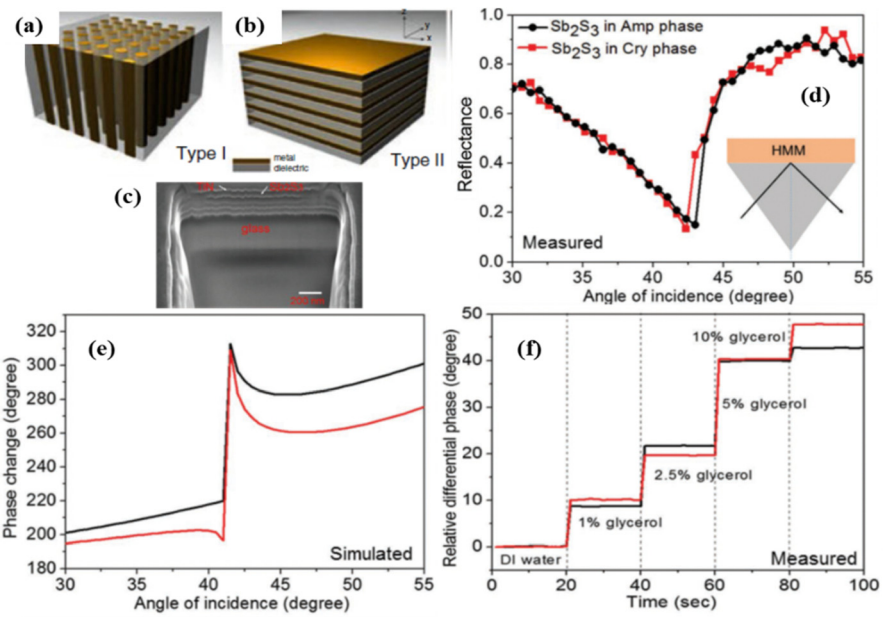

Fig. 7 Phase sensitivity in type I (a) and type II (b) hyperbolic metamaterials. Modified from ref. 151 with permission from Springer Nature, copyright 2017; (c) a scanning electron microscopy image of a HMM based on 5 pairs of Sb_2S_3-TiN layers, each having the thickness of 25 nm, 16 nm, respectively; (d) experimental angular reflectance spectrum from Sb_2S_3–TiN HMM for amorphous (black) and crystalline (red) phases of Sb_2S_3; (e) angular dependence for the simulated phase difference between TM and TE polarization components; (f) experimental dependence of differential phase signal for different weight ratios of glycerol in distilled water. Adapted from ref. 152 with permission from John Wiley and Sons, copyright 2017.

a phase-sensitive biosensor based on edge states in heterostructures containing hyperbolic metamaterials, which allows for wide-angle measurements due to the opposite wavelength shifts of edge states for orthogonal polarizations.

6.3 Ultra-high biosensitivity in periodically ordered plasmonic metamaterials enabling surface lattice resonances

These metamaterials are based on periodic arrays of plasmonic nanostructures (nanoparticles, nanostripes, *etc.*), which can enable diffractive coupling of localized plasmon resonances over the entire nanostructure,[32,33] commonly referred to as surface lattice resonances (SLRs).[40] When nanoparticles are randomly distributed, they scatter light out-of-phase and the resulting LPR is broad and not deep (Fig. 8a, the blue curve). However, when nanoparticles are arranged in an array with a period determined by the pumping wavelength and the angle of incidence, the field scattered by each particle can arrive in phase with the incident light and one diffracted wave propagates over the array (inset of Fig. 8a). If the parameters of the array (nanoparticle size and shape, lattice period) are properly selected, the diffracted wave can electromagnetically couple LPRs from individual nanoparticles, leading to a drastic narrowing of resonances in transmission or reflection (down to a few nm), as shown in Fig. 8a (the magenta curve), useful in many applications.[40–42] More importantly, under certain parameters of arrays SLRs can exhibit nearly zero intensity in the resonance minimum and related singularities of light phase, opening access to extreme phase sensitivity.[32,33] Fig. 8b shows the amplitude and phase characteristics of light reflected from 320 nm period arrays of glass-supported 118 nm gold nanoparticles. The excitation of SLRs results in a drastic drop of intensity at the resonance (within 1% compared to off-resonance

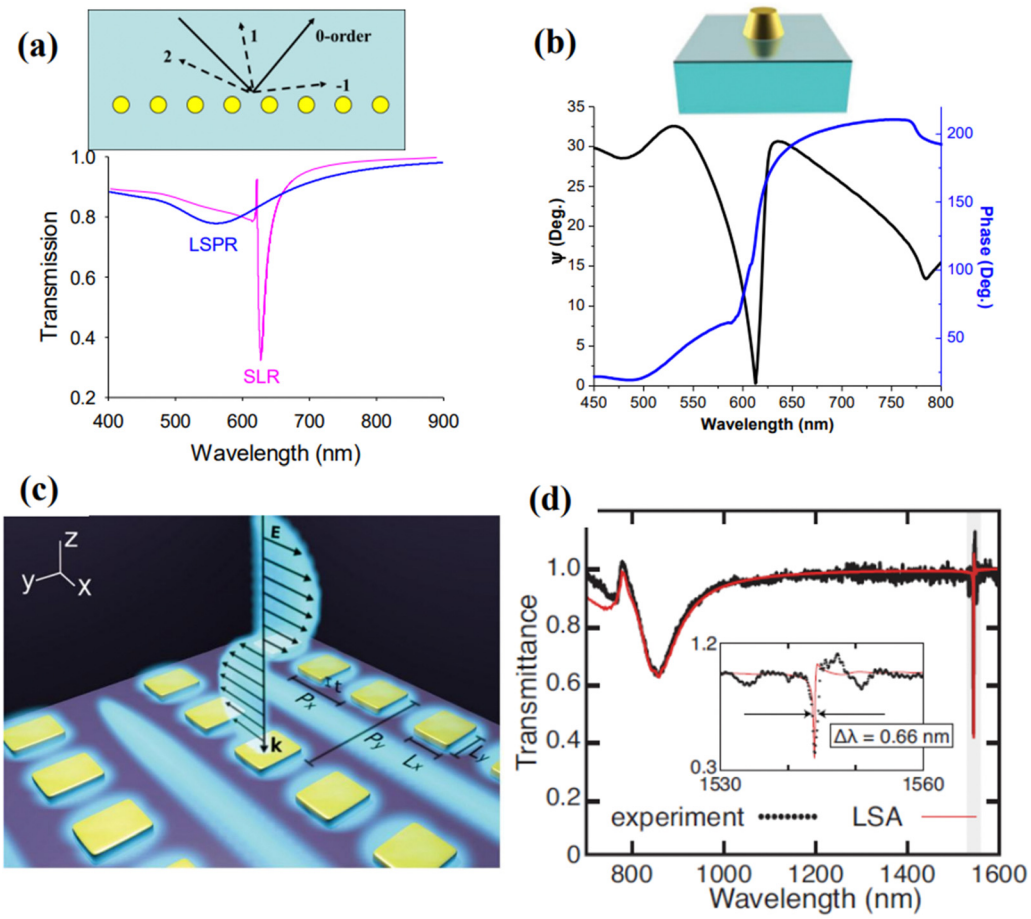

Fig. 8 Light transformations and surface lattice resonance (SLR) in periodically ordered plasmonic metamaterials: (a) effect of diffraction-coupled SLR. Calculated spectral dependences for normal light transmission for randomly distributed 80 nm Au particles and the same nanoparticles arranged in a periodic 1D array (periodicity 620 nm, 1000 nanoparticles in the array). The inset shows schematically diffraction orders from a periodic array of nanoparticles. Under certain conditions, a wave corresponding to one diffraction order can propagate over the array plane. Adapted from ref. 40 with permission from American Chemical Society, copyright 2018; (b) spectral dependencies of ellipsometric reflectivity Ψ (black) and phase Δ (blue) for a 320 nm period arrays of glass-supported 118 nm gold nanoparticles arranged in a single particle array, incident angle of 71.2°. Adapted from ref. 33 with permission from Springer Nature, copyright 2013; (c) design of nanocavity metasurfaces based on an array of rectangular gold nanostructures, providing extremely high quality of SLR; (d) measured transmission spectrum and its fits (red line) of the structure shown in panel (c). The Inset shows zoomed plot of the highlighted region. The fitting provides a linewidth of $\Delta\lambda$ = 0.66 nm, corresponding to the quality factor of Q = 2340. Adapted from ref. 154 with permission from Springer Nature, copyright 2021.

conditions) and the generation of a phase singularity in the very resonance minimum.

Kravets *et al.*[32] described several designs of single and double nanoparticle arrays, which provided phase singularities *via* the excitation of diffraction coupled SLRs. The recorded phase sensitivity, measured with a standard glycerol–water mixture calibration model, exceeded 10^6 deg RIU^{-1}, giving access to an unprecedented sub-10^{-9} RIU detection limit level. Using a model of reversible hydrogenation of graphene deposited on an array of Au nanoparticles, Kravets *et al.*[33] quantified the areal mass sensitivity of such nanotransducers and estimated the detection limit to be at the level of $\sim$0.1 fg mm^{-2}. This is many orders of magnitude better than reported in literature for LPR[15] and SPR,[14] respectively, as well as 300-fold better than reported for an alternative label-free technique based on whispering gallery modes ($\sim$30 fg mm^{-2}).[9] Using a well-developed and calibrated protocol based on the streptavidin–biotin affinity, Kravets *et al.*[33,157] experimentally showed the possibility of areal mass sensitivity of less than 1 fg mm^{-2}, which corresponded to the attachment of a single streptavidin molecule per gold nanoparticle in the array, promising single molecular level in a simple label-free optical detection.

The development of SLRs in periodically ordered plasmonic metamaterials has recently become a hot topic resulting in the introduction of a series of novel designs providing extremely high-quality resonances.[40–42,154,156,158] In particular, arrays of metasurface cavities described by Saad Bin-Alam *et al.*[154] demonstrated unprecedented resonance quality reaching Q = 2340 (Fig. 8c and d), which look extremely promising for the development of future biosensor devices, including phase-sensitive designs. In another study, Wang *et al.*[156] recently demonstrated a biosensor design based on a plasmonic crescent nanoarray, which is capable of generating SLRs with an exceptionally high FOM of a sensing response. As follows from Fig. 9a, such arrays can provide Fano-like resonances with two peaks (peak1 and peak2) and a characteristic dip (valley), while the maximal electric field is generated in valley region (Fig. 9b–e). As shown in Fig. 9f and g, such a sensor can combine a relatively high spectral sensitivity to RI changes (>1000 nm RIU^{-1}) and a very high FOM exceeding 120. The same study reports the possibility of generating FOM higher than 1800 by optimizing the nanocrescent array design, although such a FOM is accompanied by a lower spectral sensitivity. We believe that such arrays can provide even better properties when phase interrogation is used to characterize refractive index changes instead of using intensity. A recent work has also observed SLRs in dielectric arrays (dielectric metasurfaces). These SLRs are sometimes termed guided mode resonances and they could also provide extreme phase sensitivity. Barth *et al.* experimentally demonstrated the label-free phase detection of procalcitonin (a small protein of

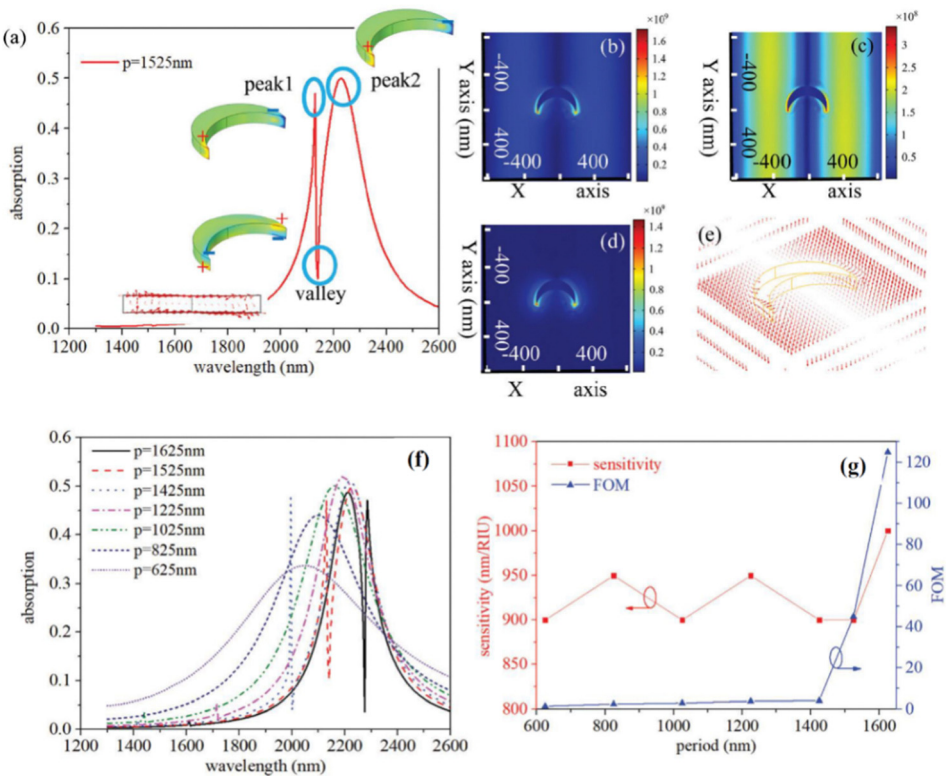

Fig. 9 High figure-of-merit plasmonic crescent nanoarray-based sensor. (a) Excitation of Fano-like SLR using plasmonic crescent nanoarrays with a lattice constant of 1525 nm. Inset illustrates charge distribution with zero charge value indicated by green color pattern; Normalized electric field distribution of peak1 (b), valley (c) and peak2 (d), respectively. (e) Distribution of electric field in the valley region; Absorption spectra (f) and sensing responses (sensitivity and FOM) for crescent nanoarray-based sensors with different lattice constants (g). Adapted from ref. 156 with permission from Royal Society of Chemistry, copyright 2022.

13 kDA and a biomarker for infection)[159] at the clinically relevant concentration of 1 pg mL^{-1} using guided-mode resonances in a regular 1D array of Si_3N_4 stripes deposited on SiO_2 substrate. A common path interferometer (based on TM and TE modes of excitation) was employed in this research so that the shift of an interferogram happening during a bio-reaction could be studied. This clever design allows one to achieve an unimpeded operation of biosensor at different concentrations of bio-analytes, helping to resolve the important trade-off between high sensitivity and small dynamic range of sensor operation. The authors hope that their design will open up possibilities for detecting clinically or environmentally relevant small molecules using a simple setup.

6.4 Fourier nanotransducers based on periodic structures to enable ultimate bio-sensitivity

Kabashin *et al.*[38] recently showed that phase singularities and related phase supersensitivity can be obtained with particular light transformations in periodically ordered metamaterial structures. These metamaterials were termed "Fourier metamaterials" to emphasize the key role of array periodicity in the generation of phase singularities (Fig. 10). In general, light scattered by a biosensor transducer contains almost all information about the transducer dynamic state (*e.g.*, refractive index of biological layer contacting the metal), but this information is distributed evenly among all possible Fourier components of light observed in the far-field. However, under some conditions, this information can be accumulated in the light confined by the transducer and then encoded in just a few coherent optical beams (reflected, transmitted, and diffracted) produced by a periodic nanostructure design. Fourier nanotransducers were introduced as sensor transducers, which are capable of confining light in a 2D plane in contact with an ultrathin biological layer of interest to gather time-resolved information on its optical properties (variations of refractive

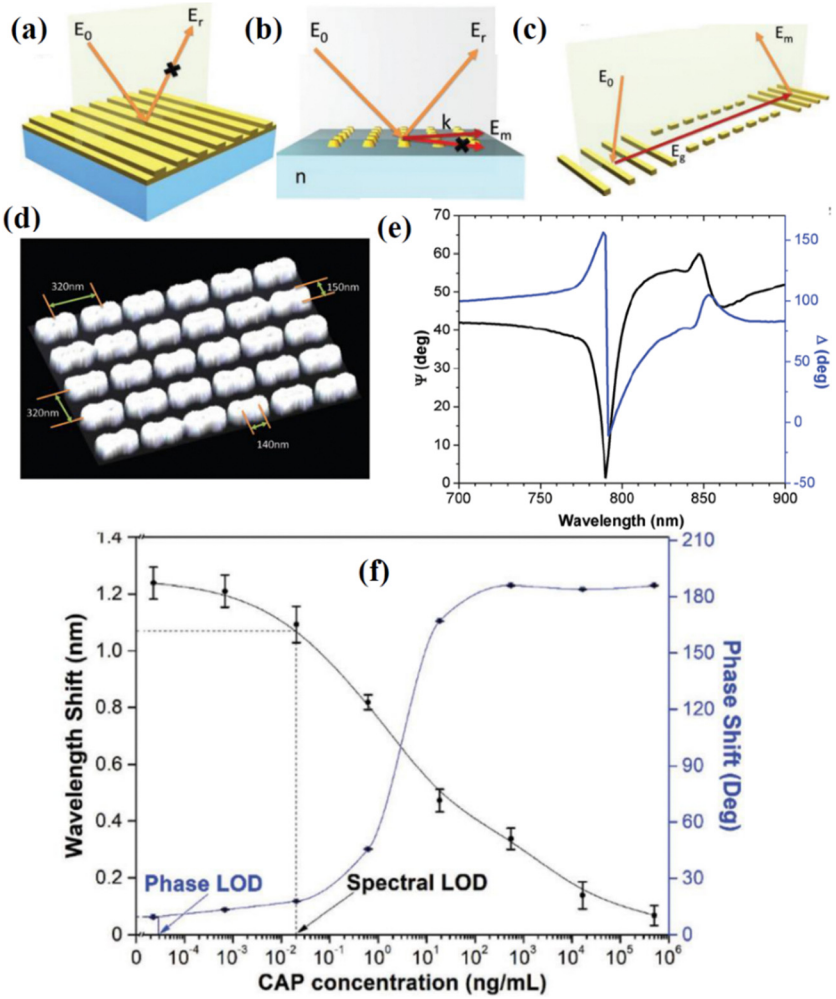

Fig. 10 Phase-responding Fourier nanotransducers. Phenomena in periodically ordered metamaterials, leading to nearly zero reflection and a related singularity of light phase: (a) drastic drop of intensity in reflected, transmitted, or diffracted beams due to absorption; (b) disappearance of a diffraction order (Rayleigh cut-off) or a redistribution of energy between them; (c) light coupling to a guiding mode; (d) example of Fourier metamaterial based on an array of merged 150 nm plasmonic nanoparticles; (e) ellipsometric reflectivity Ψ (black) and phase Δ (dark blue) for light reflected from the array from panel (f) under its contact with aqueous ambience in ATR geometry (f) dependence of spectral resonance minimum position (black) and light phase signal (dark blue) on concentration of chloramphenicol (CAP) measured using the array from panel (d). Adapted from ref. 38 with permission from John Wiley and Sons, copyright 2019.

index or selective bio-reaction), and then transmitting the information into discrete optical beams with amplified phase relations.[38] The hypersensitivity of such nanotransducers is due to the combination of the singular phase behaviour arising near complete light darkness at the resonant conditions and the strong localization of electric field at the probed biological layer. Kabashin *et al.*[38] also described the physical phenomena in such nanotransducers that can lead to phase singularities and related hypersensitivity: (i) a sudden drop of intensity in reflected or other beams due to absorption in the system or other effects (Fig. 10a), (ii) the disappearance of diffraction orders (Fig. 10b), (iii) the excitation of guided modes over nanostructured elements of the metamaterial (Fig. 10c). It is important to stress that the above-stated phenomena can be realized simultaneously under a proper design of periodic nanoparticle or nanostripe arrays. It is also worth noting that phase-sensitive diffraction-coupled SLRs could be considered as one of implementations of Fourier nanotransducers.

To explore the potential of Fourier nanotransducers in biomedical tasks, Kabashin *et al.*[38] fabricated 2D nanoparticle arrays (Fig. 10d) combining the generation of grazing beams and disappearance of diffraction orders in the attenuated total reflection geometry, which provides a nearly complete light darkness at the resonance and the generation of an extreme phase singularity (Fig. 10e). The nanotransducers were tested in a commercial ellipsometer system to detect low molecular weight molecule chloramphenicol (CAP), an antibiotic with a broad spectrum of action, which is used for clinical treatment of ocular, ear, and skin infections and in veterinary medicine. Sensing was performed in a competitive mode, in which the CAP analyte in a sample under investigation was preincubated with anti-CAP antibody and the incubated complex was pumped near CAP-coated Au nanoparticles. As shown in Fig. 10f, the decrease of CAP concentration in the complex led to a change of spectral position of the resonance and its phase. Here, the spectral parameter came to saturation at a relatively high CAP concentration, conditioning the minimal concentration of 25 pg mL^{-1} (determined *via* the 3σ criterion), which was comparable with the best values reported in the literature. At the same time, the phase started to saturate at several orders of magnitude lower concentrations conditioning the relevant LOD at the level of 27 fg mL^{-1}, which is almost three orders of magnitude better than all values recorded by alternative label-based or label-free techniques. It was suggested that alternative low-noisy phase detection implementations could improve the detection limit to below 1 fg mL^{-1}, promising a breakthrough in the advancement of label-free biodetection technology.

Remarkably, Fourier nanotransducers, which enable the manipulation of diffracted light *via* an appropriate design of periodically ordered nanostructured arrays, have been seen as a major advancement for last years under a different guise (albeit being termed differently). Recently, Overvig and Alù[160] called this class of metamaterials "diffractive nonlocal metasurfaces" and summarized developments in this field by describing a series of novel designs (plasmonic, dielectric, bianisotropic, *etc.*) having different degrees of nonlocality and providing a controlled optical response (Fig. 11). Although the main focus

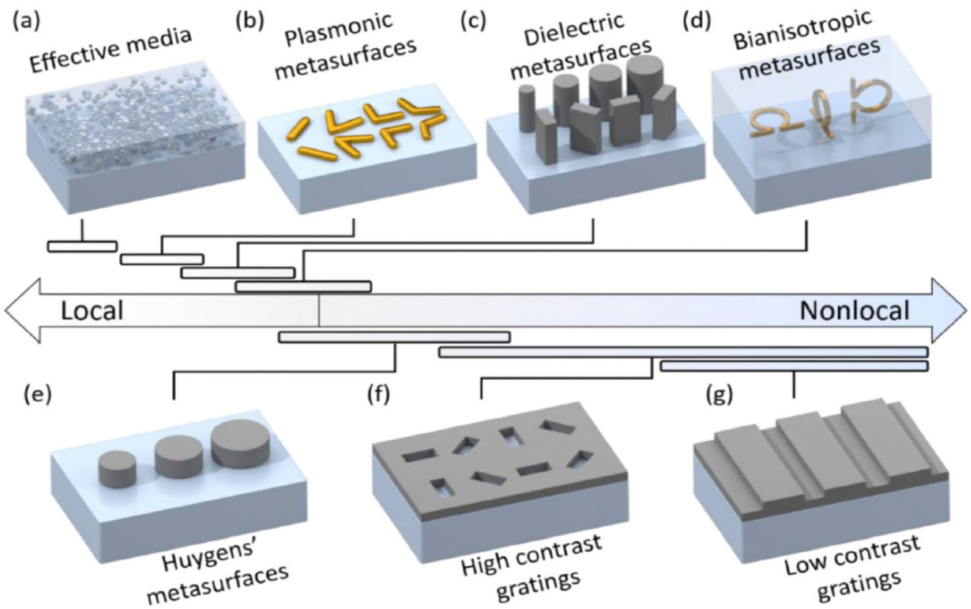

Fig. 11 Diffractive nonlocal metasurfaces arranged according to different degrees of nonlocality. (a) Effective media comprising nanoscale inclusions simulating optical properties of thin films; (b) plasmonic metasurfaces based on nanoscale antennas, providing local optical responses; (c) dielectric metasurfaces; (d) bianisotropic metasurfaces allowing manipulation of electric and magnetic dipole components and thus providing an angle-dependent response; (e) Huygens' metasurfaces rendering possible two angle-dependent resonances to manipulate forward scattered light; (f) high contrast gratings composed of high contrast regular lattices, whose nonlocality can be controlled by band structure and *Q*-factor engineering. (g) Low contrast gratings composed of shallow corrugations. Reproduced from ref. 160 with permission from John Wiley and Sons, copyright 2022.

in the development of such structures was related to light tailoring and the development of flat optics, we believe that they present great promise for the development of future designs of ultrasensitive optical biosensors, including phase-sensitive implementations.

6.5 Biosensing in 2D and 3D plasmonic metamaterials enabling topological darkness – work in the progress

Another method of realizing phase singularities and extremely high phase sensitivity is based on the phenomenon of topological darkness (TD). TD can be realized using properly designed nanostructured or/and heterostructured plasmonic metamaterial arrays (periodic or aperiodic), providing optical constants intersecting with the zero reflection curve according to the diagram of Fig. 12a.[36] In the case of TD, the crossing point is topologically protected by Jordan theorem;[33] sample imperfections do not change the fact that the two curves (the zero reflection curve and the spectral curve of effective optical constants of the nanostructured layer $n(\lambda)$, $k(\lambda)$) will cross each other and hence TD survives in the presence of sample imperfections. This becomes especially clear if we consider the properties of TD in the 3D space of (n, k, λ).[36,161,162] Song *et al.* introduced a surface of zero reflection generated at different incident angles due to the nature of the Fresnel reflection coefficients,[161] see Fig. 12b. If the effective constants of the bio-sensitive layer show resonances and intersect the surface of zero reflection, then the point of intersection becomes topologically protected[33] so that small imperfections

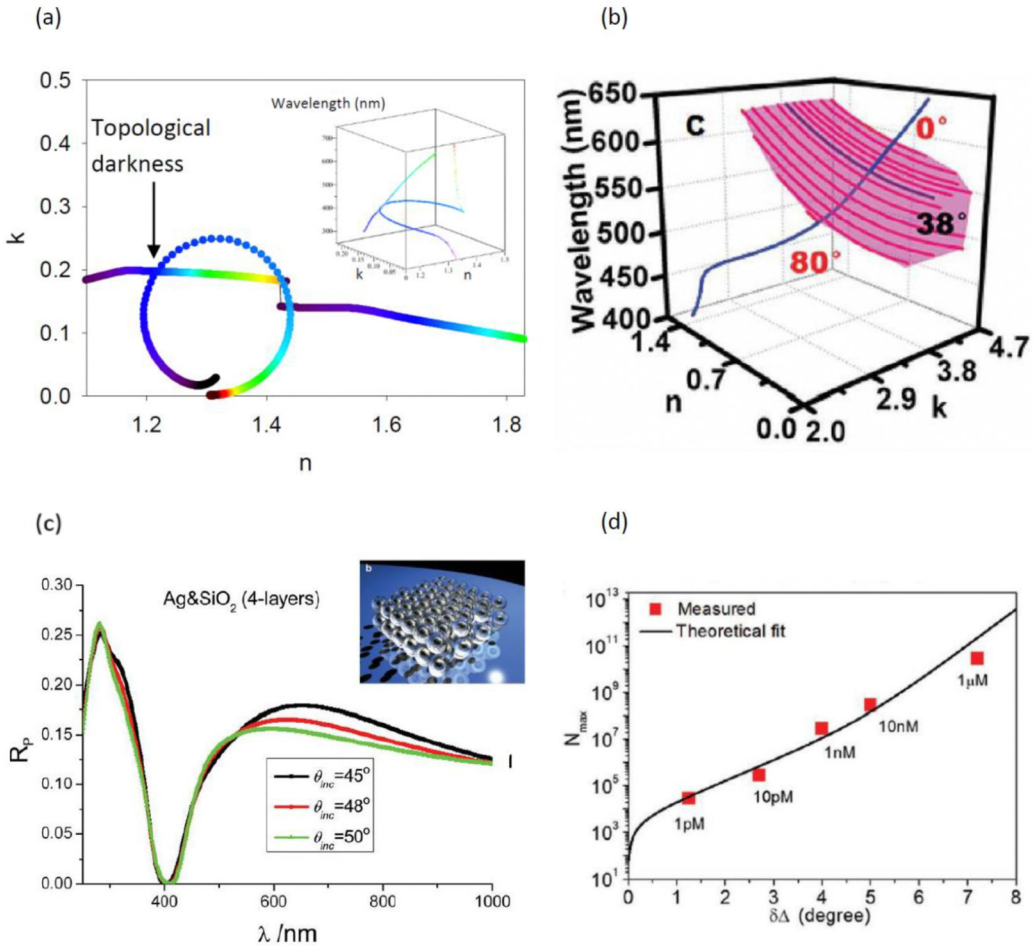

Fig. 12 Topological darkness in nanostructured metamaterials. (a) 3D picture of topological darkness explained in terms of 2D curves. Adapted from ref. 36 with permission from John Wiley and Sons, copyright 2014; (b) TD in 3D space of (n, k, λ). The Fresnel coefficients generate the zero reflection surface shown by pink color (produced by the zero reflection curves at different angles). The blue curve shows the spectral dependence of the optical constants of nanostructured metal. This curve intersects the zero reflection surface at an incident angle of 38° and wavelength ~570 nm resulting in a topologically protected zero reflection point (the spectral curve still intersects the surface of the zero reflection even in the presence of imperfections). Adapted from ref. 161 with permission from John Wiley and Sons, copyright 2017; (c) reflection of p-polarized light from 3D metamaterials with a point of TD at 400 nm. The metamaterial is made of Ag/Si meta-atoms shown in the top inset. Adapted from ref. 36 with permission from John Wiley and Sons, copyright 2014; (d) detection of biotin by an Au(20 nm)/MMA(520 nm)/Ge(10 nm)/Ag(80 nm) functionalized heterostructure. The plot shows the maximum number of biotin molecules (N_{max}) adsorbed in the illuminated sensor area *versus* the corresponding phase shift ($\delta\Delta$). The black curve is the best-fit function. The error bars are represented by the size of the data points. Adapted from ref. 61 with permission from John Wiley and Sons, copyright 2019.

in the structure design do not change the fact of the intersection and the system still shows exactly zero reflection (albeit at slightly different angle and wavelength). It is worth mentioning that TD is quite a general phenomenon and can be observed in both 2D structures (metasurfaces) and 3D structures (metamaterials). Fig. 12c demonstrates zero reflection for an artificial 3D metamaterial made of Ag/Si meta-atoms shown in the inset of Fig. 12c. The zero reflection in this case is observed near 400 nm for p-polarized light (and 420 nm for s-polarized light, not shown here). In another study,[163] TD was realized using a 3D plasmonic crystal metamaterial based on 3D periodic woodpile arrays (period d = 650–750 nm) fabricated by direct laser writing (DLW) using multi-photon polymerization, followed by Ag-based electroless plating. It is interesting that the recorded spectral sensitivity (2600 nm RIU^{-1}) was much higher than the sensitivity expected from the structure periodicity ($\Delta\lambda/\Delta n \sim d$)[39] and thus outperformed the relevant parameters for all 2D periodic arrays. On the other hand, 3D plasmon crystal structures demonstrated a high phase sensitivity of 3×10^4 deg of phase shift per RIU change. Combined with a large surface for bioimmobilizations offered by the 3D woodpile matrix, the proposed sensor architecture looks very promising for further sensing adaptations.

Points of TD are accompanied by sharp phase changes and hence can be used for extremely sensitive phase biosensing. Being a recent concept, TD was mainly employed to detect a biotin–streptavidin reaction that is widely used as a benchmark reaction for biosensing. Nanostructured topologically dark materials showed surface mass sensitivity of 10 fg mm^{-2} in biotin–streptavidin detection for commercial installations used in the experiments, with the possibility to improve the surface sensitivity to the level of 100 ag mm^{-2} in case of dedicated phase detection schemes.[33] Sreekanth *et al.* used metal-dielectric heterostructures with TD to demonstrate 1 pM detection of the streptavidin for a biotin-functionalized surface,[61,164] see Fig. 12d. An extended discussion of topologically protected points of darkness and extreme phase sensitivity for composite heterostructures can be found in the book.[165]

Coupled metamaterial-based transducers have all the necessary attributes (simplicity of use, extremely high bio-sensitivity, relative cheapness of production) to become the new workhorses of label-free optical biosensing. In such transducers, bio-analysis (detection of viruses, antibiotic, vitamins, drugs, *etc.*) could be performed in real time at the point-of-care or point-of-action, drastically reducing the time necessary for medical or societal actions.

7. Development of novel detection architectures: Goos–Hänchen effect

Goos–Hänchen (G–H) shifts have recently attracted much attention as a new means of extracting phase information in optical biosensing devices.[132,166,167] The Goos–Hänchen effect is related to a small lateral shift of a beam reflection position predicted by geometrical optics under total internal reflection.[168,169] The shift is perpendicular to the direction of propagation in the plane containing the incident and reflected beams. The Goos–Hänchen effect is caused by penetration of incident light into the second medium (that is less dense in comparison to first, $n_1 > n_2$), which leads to the generation of an evanescent wave propagating along the interface of two media over a certain distance before re-entering the first medium (Fig. 13a). The G–H shift is directly related to variations of the phase of reflected beam and in the stationary phase approach can be described as $S = (1/k)(\partial\phi/\partial\theta)$, where k is the wave vector of light in the incident medium and ϕ is the reflected phase and θ is the angle of light incidence.[168] Since the shift is very sensitive to any variation of RI over the interface leading to a sharp variation of the optical phase signal, it can be used as phase-sensitive parameter in biosensing.

Under the condition of total internal reflection from a single dielectric interface, G–H shifts are relatively small (of the order of the wavelength of pumping light), which makes them of limited use for biosensing applications. However, since G–H shifts are directly related to the steepness of phase variations, they can be drastically amplified by the use of optical phenomena, providing light darkness under resonant conditions. One straightforward way to amplify G–H shifts is to use layered geometries,[170–172] although the amplification factor is still limited due to the difficulty of achieving complete light darkness. A more radical way to amplify G–H shifts uses hetero-metasurfaces or metamaterials, rendering possible light darkness due to enhanced absorption or other phenomena. In particular, Wang *et al.*[132] used an atomically thin $Ge_2Sb_2Te_5$ (GST) layer (with high absorption in visible and near-infrared wavelengths) deposited on the top of a Au thin film in the Turbadar–Kretschmann–Raether geometry (Fig. 13b, inset) and achieved nearly zero-refection by optimizing the thickness of the absorbing layer. The authors observed extremely sharp phase changes at the resonance angle, accompanied by a strong shift of G–H lateral position. The differential G–H shift between p-polarized light and unaffected s-polarized light was then recorded as the optical characteristic carrying phase-sensitive information on biomolecular interactions on the gold film. As a result, a much larger G–H shift for GST layers on gold compared to the pure gold case was observed (Fig. 13b), which was attributed to the phenomenon of light darkness described in previous sections. In addition, coating the Au surface by GST led to an amplified response of G–H shift to RI bulk variations (Fig. 13c), which confirmed the efficiency of hetero-metasurface architectures in designing hypersensitive plasmonic biosensing transducers. Other hetero-metasurface geometries that drastically amplify the G–H shift include a bimetal Ag–Au structure covered by a graphene-hexagonal boron nitride (graphene-hBN) layer,[173] hybrid metastructures based on a plasmonic film-supported two-dimensional perovskite film sandwiched between hBN and graphene layers,[174] Au-MoS_2/graphene,[175] Au-ITO-MoS_2/graphene,[176] a Dirac semimetal/graphene coupling structure,[167] *etc.* In all these cases, large G–H shifts of up to several hundred μm were reported, while the sensitivities of such G–H shift phase-sensitive transducers

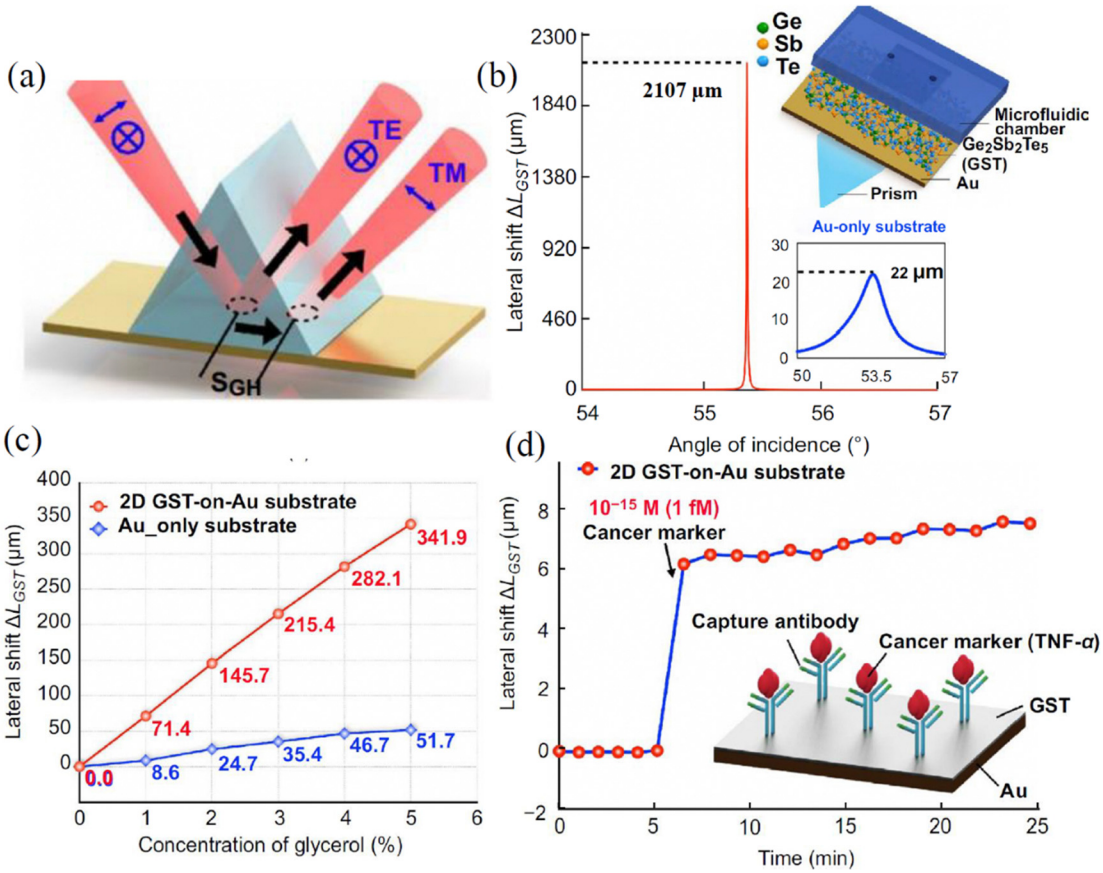

Fig. 13 Phase-sensitive hetero-metasurface-based biosensor using Goos–Hänchen effect. (a) Schematic presentation of a large lateral position shift induced by the Goos–Hänchen effect; (b) schematic of hetero-metasurface substrate based on $Ge_2Sb_2Te_5$ (GST) layers on a gold film (upper inset). Simulated angular dependence of G–H shift. The value of the shift reached 2107 μm at the resonant angle, which is much larger than the relevant value for a pure gold film in the SPR geometry (lower inset); (c) G–H shifts for GST-coated and uncoated Au substrates after the injection of glycerol solutions with different RI; (d) detection of 1 fM concentration of cancer marker TNF-α using 2D GST-on-Au substrate. Adapted from ref. 132 with permission from Springer Nature, copyright 2021.

could reach 10^5–10^6 λ RIU^{-1}. G–H shifts can be also greatly enhanced in nanostructured metamaterials that enable the light darkness phenomenon. A variety of such metamaterials were recently proposed, including a nanophotonic asymmetric Fabry–Perot cavity near Brewster's angle,[177] a multi-layer hyperbolic metasurface[62] or a metasurface with a nanogroove structure,[166] symmetric metal cladding plasmonic waveguide (SMCW) structures,[105] a subwavelength grating metamaterial (SGM) waveguide,[178] *etc.* The reported G–H shifts and sensitivities for nanoscale metamaterials roughly correspond to the relevant parameters obtained with their hetero-metasurface counterparts, suggesting that the presence of light darkness is a key parameter to achieve extreme sensitivity based on the G–H effect and this result can be achieved *via* the use of both hetero-metastructures and nanostructured metamaterials.

Optical biosensors based on G–H shifts have already been tested in biomedical tasks and demonstrated high efficiency. In particular, using hetero-metasurface substrate based on GST layers on a gold film, Wang *et al.*[132] reported the possibility of detection of sub-attomole concentrations of for TNF-α cancer marker (Fig. 13d), which is orders of magnitude lower than LOD values obtained with their amplitude-sensitive counterparts. As another example, using silver–stibnite nanoporous plasmonic films, Sreekanth *et al.*[179] reported a LOD for the bovine serum albumin (BSA) molecule at level of 0.1×10^{-18} M, which corresponds to a submolecular detection level (0.13 BSA mm^{-2}).

In general, detection schemes based on the G–H effect have demonstrated a high efficiency in extracting the phase-sensitive response in conditions of light darkness and could be applied for most structural layouts and metamaterial architectures described in the previous sections. One potential advantage is the relative simplicity and compactness of the experimental arrangement for the control of G–H shifts.

8. Recent advances

8.1 Dielectric platforms for optical label-free biosensing

Plasmonics provides an excellent platform for concentrating light in nanoscale with promising applications in biosensing and biomedicine. Recently, however, high-refractive index

dielectric nanostructures featuring low-loss resonances have been proposed as a encouraging alternative to nanoplasmonics, potentially offering comparable or even better sensing performances.[180–182] According to the Mie theory,[183] both plasmonic and dielectric particles can possess strong scattering resonances. Due to a low level of losses in dielectrics, high-index dielectric nanoparticles of simple geometries can exhibit the electric dipole (ED) and magnetic dipole (MD) resonances of comparable strengths (Fig. 14a and b). The enhancement of MD resonances occurs when the wavelength of light inside a dielectric particle becomes comparable with the particle size. This condition can be achieved under $2R \approx \lambda/n$, where n is the refractive index of the dielectric nanoparticle, R is its radius, and λ is wavelength of light.[180–182] Moreover, for larger nanoparticles, the MD resonance becomes stronger than the ED resonance providing a major contribution to the scattering efficiency. The spectral positions of both electric and magnetic dipole resonances can be tuned independently by changing the geometrical parameters of dielectric structures; *e.g.*, Fig. 14a displays the spectral overlapping of MD and ED resonances for Si nanodiscs.

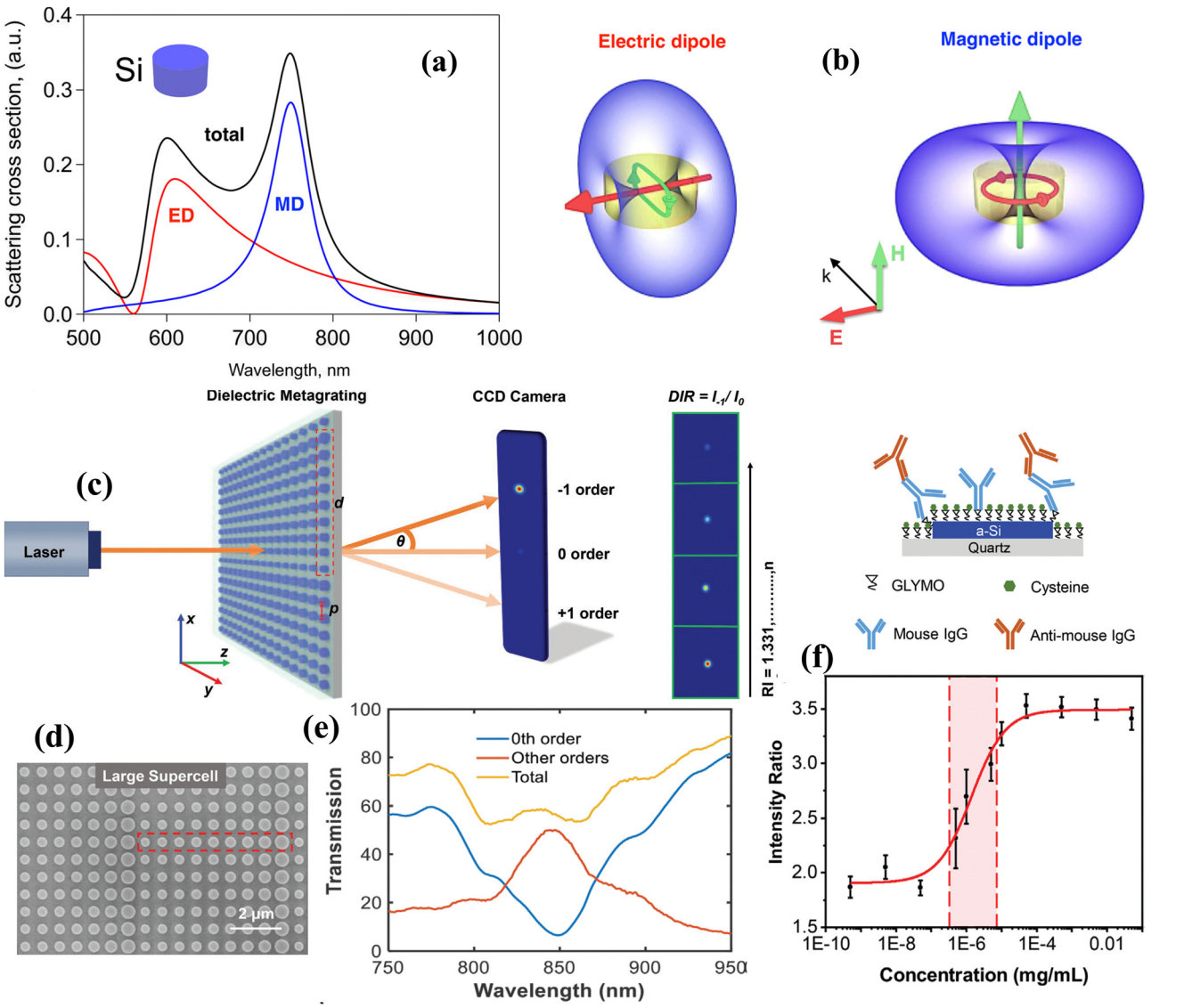

Fig. 14 Dielectric platforms for label-free optical biosensing: (a) excitation of Mie resonances. Scattering cross section of a silicon (Si) nanodisc (200 nm radius and 260 nm height). Resonances related to magnetic and electric dipoles are denoted as MD and ED, respectively; (b) configuration of fields corresponding to resonant contributions from MD and ED in Panel (a). Adapted from ref. 182 with permission from American Chemical Society, copyright 2017; (c)–(f) dielectric metagrating platform for biosensing. (c) Schematic of operation of sensor based on periodically repeated 9-nanodisk unit cells (an example of such a cell is highlighted by red dashed line) and that of signal acquisition based on the control of diffraction intensity ratio DIR = I_{-1}/I_0 as a function of RI; (d) an image of a metagrating providing a small deflection angle (SDA); (e) light transmission spectra for different diffraction orders for the SDA grating shown in panel (d); (f) biosensing experiments on anti-Mouse Immunoglobulin G (IgG) detection. Schematic of selective binding of anti-Mouse IgG (upper inset). Dependence of average intensity ratio (DIR) on concentration of anti-Mouse IgG in the solution (range of concentrations from 5×10^{-10} to 5×10^{-2} mg mL^{-1}). The red curve shows a four-parameter logistic fit. Adapted from ref. 187 with permission from John Wiley and Sons, copyright 2022.

Recently, dielectric structures and their resonances (MD in particular) were successfully used in dielectric platforms for sensitive label-free optical biosensing. As an example, a low concentration of streptavidin was detected with the help of all-dielectric nanoresonators.[184] In this study, the authors validated a new dielectric sensing platform based on silicon nanodisks with strong optically induced MD resonances, which yielded a detection limit of streptavidin at the level of 5 ng mL^{-1}. Yavas *et al.*[185] improved sensitivity of dielectric nanostructures by integrating arrays of antibody-functionalized silicon nanoresonators with microfluidics and demonstrated the detection of $\sim$1 ng mL^{-1} prostate specific antigen (PSA) in buffer. The sensing performance of dielectric Si nanodisks (a metasurface) was compared with that of gold nanorod arrays in a review article.[186] The authors showed that the dielectric metasurface possesses a better LOD compared to the plasmonic counterpart while the plasmonic nanorod metasurfaces afford a wider dynamic range.

Aoni *et al.*[187] proposed a dielectric metagrating platform for label-free optical biosensing based on an array of dielectric nanodiscs of different sizes, exhibiting individual Mie resonances. The nanodiscs were arranged in such a way that they could condition phase values from 0 to 2π in light transmitted through the structure (Fig. 14c). The whole structure presented a set of periodically repeated unit cells (highlighted by a dashed red line) to form a metagrating. The illumination of this structure by white light leads to the appearance of different diffraction orders in transmission and the intensity in these orders is conditioned by the phase ramp imprinted by the metagrating. It is critically important that under such a geometry the diffraction intensity ratio DIR = I_{-1}/I_0 (where I_{-1} and I_0 are intensities in high and zero orders, respectively) becomes highly sensitive to RI of the medium contacting the structure (Fig. 14c, right panel), which opens up access to the employment of such megagratings to control biological binding events. Depending on metagrating parameter, the structure can provide large or small deflection angles. The authors showed that smaller deflection angle (SDA) metagratings can provide better sensitive response to RI variations. An example of such SDA grating and corresponding transition spectra from different diffraction orders are shown in Fig. 14d and e. Fig. 14f (upper inset) displays the immobilisation of a primary antibody (Mouse IgG) onto a dielectric metagrating using silicon to amine/sulfhydryl coupling strategy. Testing of the sensitivity was performed with the help of an anti-Mouse IgG binding assay by measuring the diffraction intensity ratio of the 0th and -1st diffraction orders at a range of analyte concentrations from 5×10^{-10} to 5×10^{-2} mg mL^{-1}, Fig. 14f. The resulting LOD of 0.1 ng mL^{-1} for anti-Mouse IgG was achieved.[187]

We briefly mention that in addition to reflection/transmission/diffraction techniques, the fluorescence (FL) detection can be used in combination with dielectric metasurfaces.[188,189] Iwanaga *et al.*[188] suggested to employ dielectric metasurface FL sensors for the detection of COVID-19 spike protein. The enhanced intensity of FL allowed one to measure the glycoproteins and antibodies more efficiently, as compared to other methods previously reported. The FL sensors based on a dielectric metasurface demonstrated LOD less than 0.64 pg mL^{-1} for glycoprotein peptides detection and the dynamic range was more than five orders of the target concentrations.[188] The highest-sensitivity biosensing FL platform was demonstrated in ref. 189, where immunoglobulin G with concentrations of the order of pg mL^{-1} was detected.

Some efforts on developing the dielectric platform for biosensing were discussed in a recent review.[190] It is worth stressing that, despite being impressive, LODs achieved with dielectric metasurfaces and other dielectric platforms ($\sim$1 ng mL^{-1}) are well below LODs that one can achieve with plasmonic phase metamaterials ($\sim$1 fg mL^{-1}), see Fig. 2. This means that the dielectric platform could probably be further improved by employing phase as the sensing parameter at the condition of light darkness.

8.2 The concept of bound states in the continuum for highly sensitive biosensors

High-index all-dielectric metasurfaces have a disadvantage of a broad spectral response at ED and MD resonances severely restricting their LOD. It was recently found that sharp resonances could be achieved by utilising the concept of bound states in the continuum (BICs). Narrow resonances in BICs happen when light waves remain completely localized at a metasurface even though they coexist with a continuous electromagnetic spectrum of the environment.[192,193] While original BICs suggested by von Neumann and Wigner[194] are difficult to implement, there are other practical scenarios leading to the generation of BICs. For example, BICs can be realised in Fabry–Perot structures, coupled resonances (Friedrich–Wintgen (FW) BICs), parametric structures, *etc.*[192] Usually, BICs possess very high (theoretically divergent, but finite) values of the quality factor (Q) due to structural losses and imperfections.

An application of quasi-BIC resonances for biosensing was demonstrated in metasurfaces based on a dimer-type unit cell.[195] The authors performed real-time in-flow detection of biological extracellular vesicles (EVs) secreted from cancer cells with the help of an immunoassay. A quasi-BIC metasurface was integrated with a microfluidic flow channel resulting in the overall LOD of 126 ng mL^{-1}.[195] Wu *et al.*[196] implemented a BIC-based biosensor using a compound grating waveguide structure with a switchable guided resonance. Due to a high Q-factor of $\sim$7000, such a sensor provided LOD of the sucrose concentration at the level of 1.6×10^{-5} g mL^{-1}. An optical biosensor with a high quality factor, Q was engineered using the Friedrich–Wintgen type BICs.[197] This sensor is valuable in quality control analysis of food processing, for example for trace detection of a specific benchmark analyte, ochratoxyn A. Experimentally, a relatively low LOD of 2.3 pg mL^{-1} was achieved. In addition, a FW-BIC type biosensor could be applied for the detection of other mycotoxins and low-molecular weight molecules. The topological light confinement effect in a quasi-BIC resonator was employed for PNA/DNA selective biosensing with real-time monitoring of binding events.[198] Measurements of transmittance spectra before and after the incubation with c-DNA (c = 0.05 nM)

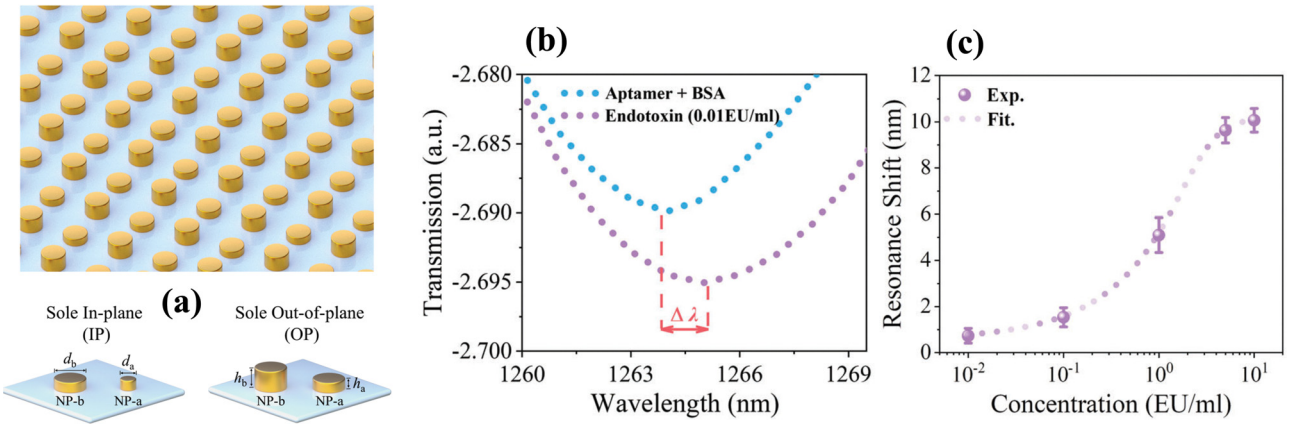

Fig. 15 Biosensor based on hetero-out-of-plane symmetry protected bound states in the continuum (BIC) metasurfaces. (a) Examples of metasurfaces with Sole In-plane (Δd) and Sole Out-of-plane (Δh) broken symmetry; (b) evolution of the position of q-BIC resonance generated in the hetero-out-of-plane (H-OP) geometry under the adsorption of endotoxin with concentration of 1 pg mL^{-1} in a buffer solution; (c) dependence of q-BIC resonance position on endotoxin concentration. Adapted from ref. 191 with permission from John Wiley and Sons, copyright 2023.

demonstrated the sensitivity of 20 molecules per μm^2. The authors expected further improvements toward the achievement of single molecule detection. Wang *et al.*[191] suggested out-of-plane architectures based on symmetry protected (SP)-BIC metasurfaces as a high sensitive biosensor. They showed that hetero-out-of-plane (H-OP, Au-SiO_2, Fig. 15a) SP-BIC metasurfaces can exhibit a robust high Q-factor resonance suitable for biosensing. Fig. 15b shows a quasi-BIC (q-BIC) resonance shift of the H-OP architecture after the adsorption of endotoxin at the concentration of 1 pg mL^{-1} in a PBS buffer solution. The experimental q-BIC resonance red-shifts with an increase of endotoxin concentration, as shown in Fig. 15c.

Kuhner *et al.*[199] designed symmetry-broken q-BICs ring structures based on a 120 nm thick amorphous silicon layer fabricated on a glass substrate using electron beam lithography and reactive ion etching. These structures demonstrated high-Q factors exceeding 500 in the red part of the visible spectrum. The bio-molecular sensing performance for asymmetric q-BICs structures was tested by the functionalisation with (3-aminopropyl) triethoxysilane (APTES), followed by the attachment of biotin molecules and binding of different concentrations of streptavidin protein. It was found that the proposed BIC platform provides polarization-invariant and tunable high-Q resonances in an ultra-compact footprint as low as 2 μm^2 resulting in LOD of 10 nM for streptavidin molecules.[199]

Yesilkoy *et al.*[200] used dielectric metasurfaces with q-BIC properties and combined them with hyperspectral imaging to develop an ultrasensitive label-free analytical platform for biosensing. In the proposed arrangement, a metasurface array was illuminated by a narrow-band tunable laser source, while transmitted light at each wavelength was recorded using a CMOS camera to examine spatially-resolved information at every pixel (Fig. 16a). Such a setup was used in combination with a metasurface architecture based on elliptical Si pairs of nanobars tilted around one of their axes (Fig. 16b). This design makes possible the excitation of BIC and q-BIC modes of collective lattice resonances at zero and non-zero (17.5°) tilting angles, respectively, while the spectral position of these resonances can be tuned by changing resonator dimensions. The authors focused their attention on q-BIC modes, which were characterized by a strong localization of both electric and magnetic fields in the outer volume of Si pairs (Fig. 16c), making them especially useful for sensing applications. The authors also assessed biosensing performance of designed q-BICs in dielectric metasurface sensors in the geometry of image-based data processing. Rabbit-derived antimouse IgG was used as a test bio-object, while an epoxysilane chemistry was used to immobilize the receptor molecules (mouse-derived IgG) onto the sensor surface (Fig. 16d). As follows from Fig. 16e and f, a low areal molecule density of less than 1×10^3 molecules per μm^2 could be detected using BIC metasurfaces with ultrasensitive hyperspectral imaging.[200] Combined with a simplicity of information readout (expensive spectrometer equipment is not needed), such technique looks very promising for ultrasensitive spatially-resolved biosensing.

Finally, we note that despite a great progress in theory and application of BICs in biosensing, the achieved LODs are still on a moderate side which is not unexpected taken into account the infancy of this approach. Again, this approach could benefit significantly from the phase interrogation.

8.3 Exceptional point platform for biosensing

Another recent advance in optical label-free biosensing is related to the phenomenon of exceptional points (EP), which appear as spectral singularities in an open system described by a non-Hermitian Hamiltonian.[201–203] EPs can appear when at least two resonant modes coalesce to become degenerate both in their resonance frequencies and loss rates. Photonic systems look very promising for the implementation of EPs, which is confirmed by the observation of this phenomenon in many optical geometries.[202] Unique spectral properties of systems with EPs were theoretically suggested for single-particle detection *via* the monitoring of frequency and linewidth splitting of resonant modes.[203] J. Wiersig *et al.*[203] used a typical non-Hermitian optical system, in which EPs could be easily

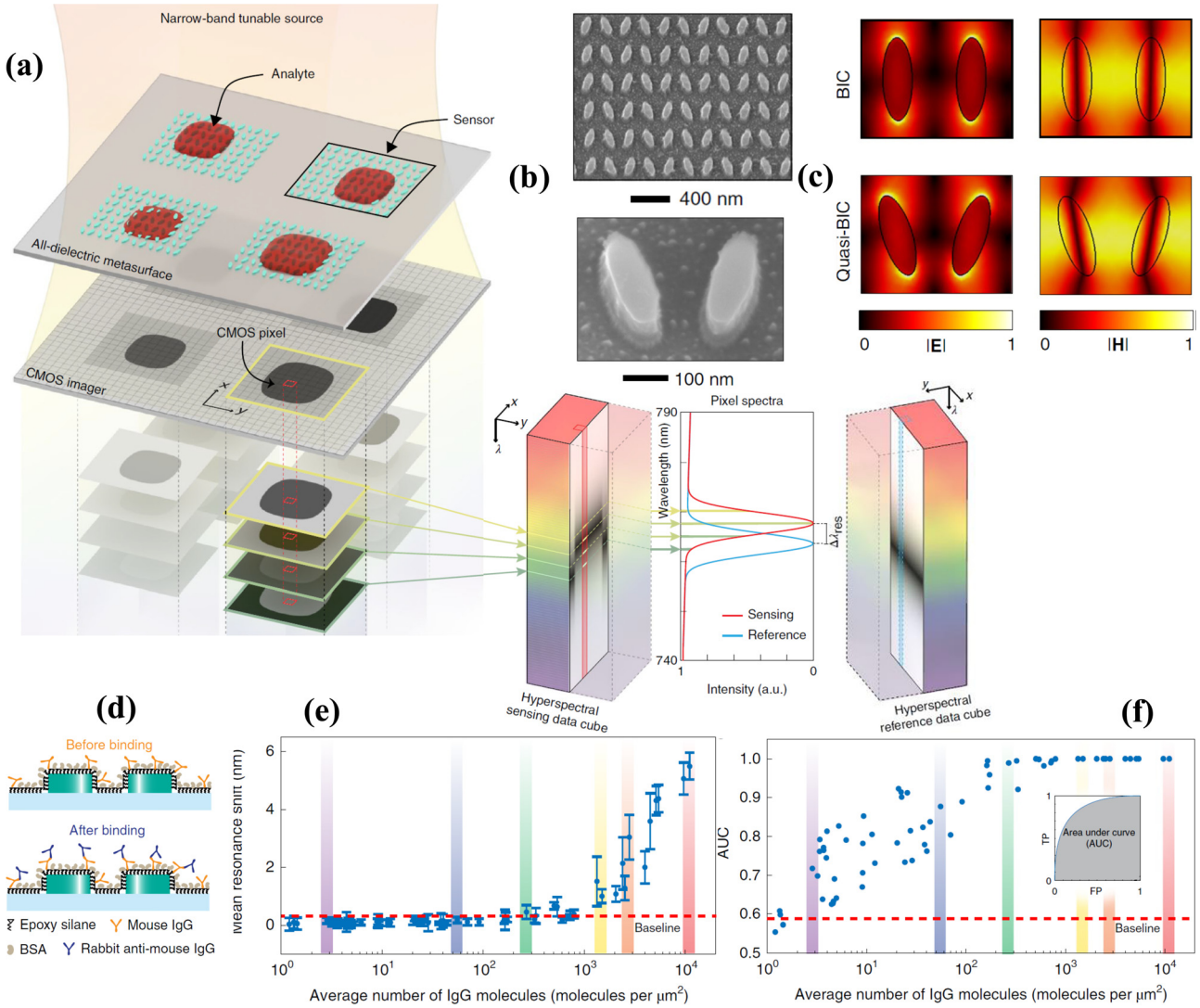

Fig. 16 Dielectric metasurfaces with q-BIC properties combined with hyperspectral imaging for highly-sensitive spatially-resolved biosensing. (a) Schematic of hyperspectral imaging scheme. An all-dielectric metasurface array is illuminated at a tuneable wavelength. A CMOS camera is then used to create a hyperspectral data cube, in which every pixel records spectral information in transmitted light; (b) SEM images of used all-dielectric metasurface composed of pairs of Si nanobars; (c) distribution of electric and magnetic fields in a pair of Si nanobars in the case of BIC and q-BIC modes. (d)–(f) Biosensing testing of metasurfaces enabling q-PIC modes in the detection of rabbit-derived antimouse immunoglobulin IgG (R-IgG). (d) Schematic of bioassay. The sensor surface is functionalized with mouse-derived IgG (M-IgG), which has a high affinity to R-IgG; (e) mean resonance shift as a function of number of R-IgG molecules. The dependence is presented in the form of a traditional calibration curve correlating the ensemble-averaged resonance shift from binding spots to the average number of R-IgG molecules per μm^2. Colour bars indicate data points associated to the resonance shift maps; (e) area under the curve (AUC) values of all receiver operating characteristic (ROC) curves. Control measurements revealed an AUC value of 0.5008 ± 0.0291 (N = 68), which gave evidence for the detection level at very low molecular counts (~3 molecules per μm^2). Adapted from ref. 200 with permission from Springer Nature, copyright 2019.

interpreted. The authors studied two coupled whispering gallery microcavity (WGM) waveguides, whose resonant frequencies, losses and gains were carefully selected to generate EPs. As WGMs utilize total internal reflection to localize light in the cavity, the resulting resonances at EPs exhibited a very high Q-factor, which is important for high-sensitive particle detection.[202,203] An improvement of sensing performance in the geometry of optical microcavity was reported in ref. 204. Here, a target molecule entering the evanescent field of the microcavity near EPs perturbed the system, leading to a frequency splitting, which could be large enough to detect a single molecule. Further improvements of optical biosensing performance can be achieved *via* the employment of a coupled system consisting of graphene plasmons (implemented in patterned graphene ribbons) and molecule vibrational modes, in which the coupling strength can be tuned from "strong" to "weak" coupling regimes yielding EPs of non-Hermitian origin.[205] The authors theoretically showed that the sensitivity of this hybrid plasmon/vibrational system to RI variations can be maximized by selecting the thicknesses of plasmonic film and the numbers

of graphene layers in the ribbons to tune the sytem to the generation of efficient EPs. Bin Liu *et al.*[206] proposed a biosensing design based on a microtube cavity having multiple layers, in which the coupling of modes can be tailored to generate EPs by a careful selection of layer thicknesses. It was theoretically shown that the proposed biosensor design could provide the improvement of sensitivity up to 1000-fold compared to conventional methods. A label-free optical biosensor based on optical tunnelling was theoretically suggested in ref. 207. The calculated LOD for the system was found to be 0.9 ng mL^{-1}. The authors envisaged the application of this biosensor based on EP metamaterial modes in environment protection, drinking water safety, and drug screening.

Park *et al.*[208] reported the observation of EPs in plasmonic systems, which looks especially promising for the implementation of biosensing devices. The authors used a bilayer periodic plasmonic structure (metallo-dielectric photonic crystal) made of two optically dissimilar plasmonic resonators (Fig. 17). The detuning of resonances in such a system was achieved *via* an out-of-plane symmetry breaking using identical resonators in distinct optical environments, as shown in Fig. 17a and b (alternatively, the detuning can be done using plasmonic nanostructures of different size in a uniform optical environment). The authors showed that in the case of optically identical resonators the generation of EPs is impossible and hybridized resonances cross along a diabolic line (at so-called diabolic points, DP) as a function of d_x and P_y. In contrast, in the case of optically dissimilar resonators one can obtain hybrid modes with crossing and avoided crossing of both the resonances and loss rates, which yields the generation of plasmonic EP where resonances and loss rates become simultaneously degenerate (Fig. 17c). It was also concluded from calculations and experiments that the biosensor operating around an EP and DP exhibits a resonance splitting ($\Delta\omega$)

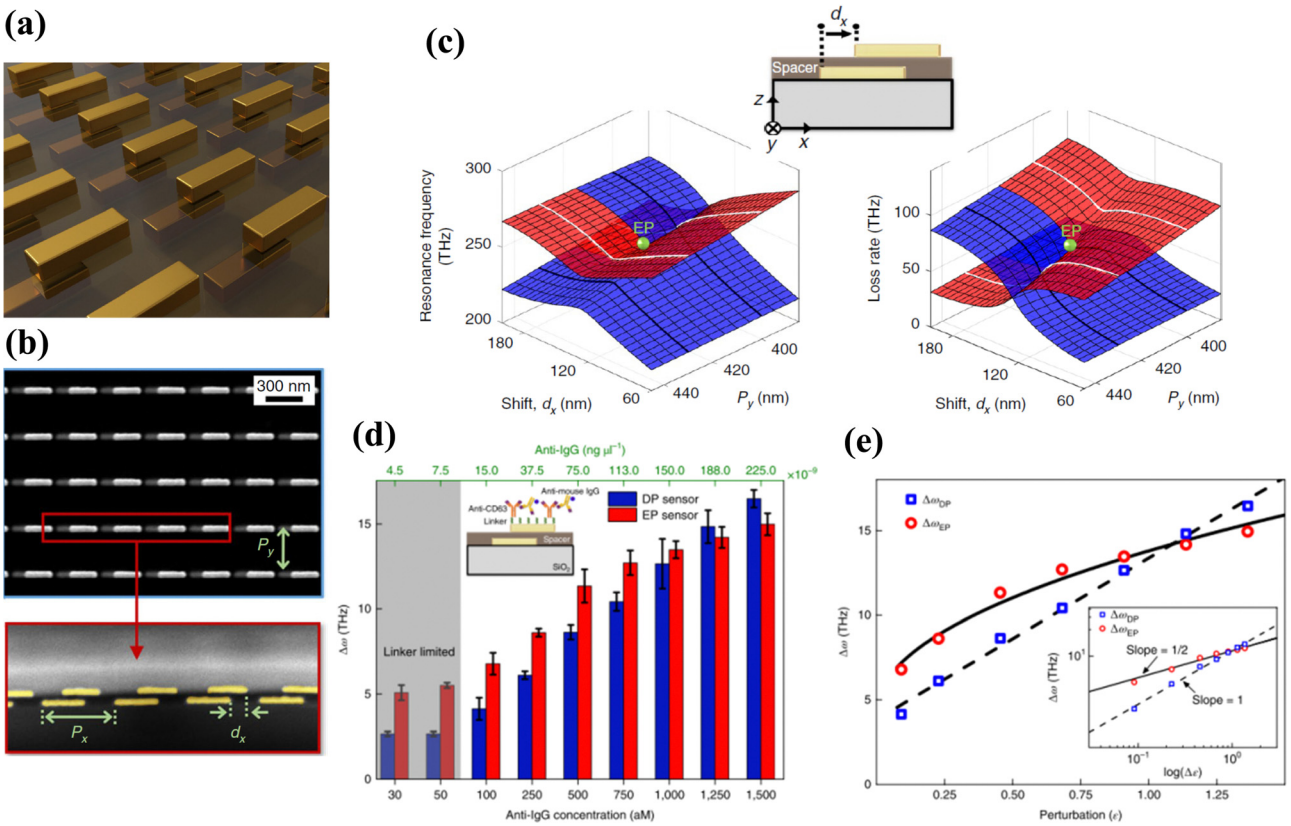

Fig. 17 Implementation of EPs in multi-layered plasmon system and their biosensing assessment. (a) Schematic of a bilayer metallo-dielectric photonic crystal made of two optically dissimilar plasmonic resonators. The resonances are detuned *via* the employment of identical plasmonic resonators based on gold metallic bars (length 250 nm, width 50 nm, thickness 40 nm) placed in two different optical environments (air and polymer SU-8); (b) Top (upper) and side (lower) views of the used metallo-dielectric photonic crystal. The period along the x direction is fixed to P_x = 400 nm while P_y and d_x are the two parameters used to reach an EP; (c) real and imaginary parts of the eigenmodes (red and blue) of hybridized plasmonic resonators arrays of identical size (in different environments), shown in panel (b), as a function of P_y and d_x. At some point corresponding to the generation of EP (green dot), the hybridization of optically dissimilar resonators provides two hybrid modes with crossing and avoided crossing of both the resonances and loss rates, and resonances and loss rates become simultaneously degenerate. (d) and (e) Immuno-assay biosensing using plasmonic EPs and diabolic points (DPs). (b) Dependence of resonance splitting $\Delta\omega$ in EP and DP sensors on anti-mouse IgG concentration. The inset demonstrated a functionalization strategy using a linker and a mouse IgG as a receptor. One can see that the EP are more sensitive than DPs under small anti-IgG concentrations. (e) Dependence of resonance splitting $\Delta\omega$ on the perturbation ε = (anti-IgG concentration aM)/(1100 aM) for the EP and DP sensors. One can see a square-root and linear dependence of resonance splitting on IgG concentration for the EP and DP sensors, respectively. Adapted from ref. 208 with permission from Springer Nature, copyright 2020.

proportional to the square root and linear value of the perturbation, respectively.[208] The authors demonstrated that suggested nanoantenna arrays with EP enables enhanced sensing of anti-immunoglobulin G (IgG). Data in Fig. 17d and e show the sensitivity to low concentrations of anti-mouse IgG for two sensors based on plasmonic EP and DP modes. Here, designed plasmonic EP nanoantenna arrays demonstrated LOD of 15 fg mL^{-1} which is better than many available plasmonic biosensor platforms.

8.4 Label-free optical detection of single molecules

Finally, we briefly discuss the problem of label-free optical detection of single molecules. The conciseness of discussion will be connected to the fact that: (i) excellent reviews on the subject already exist;[209,210] (ii) it is difficult to currently envisage how this technology could be widely employed in biomedical diagnostics, environment and food safety, security and health applications. Single molecule detection (SMD) could serve for many important tasks, including the control of molecular (digital) binding kinetics, monitoring of dynamics and constants of cells, quantification of exosomes, and the investigation of motor protein functions, detection of drugs, *etc.* SMD is typically based on microscopy modalities, which limits its usage to laboratory environment. However, SMD provides an ultimate sensitivity level in biosensing and hence deserves a brief overview.

One of the most promising microscopies for SMD is based on SPR imaging technology.[23] SPR imaging was recently significantly upgraded by the emergence of plasmonic scattering microscopy, which was then successfully applied for the detection of different analytes yielding LODs at a single-protein level.[211] While traditional SPR imaging systems measure the intensity of reflected light, plasmonic scattering microscopy deals with out-of-plane scattered surface plasmonic waves produced as the result of the interaction of plasmonic system with analytes. The authors claimed that their method allows one to achieve a SPR imaging option with high spatiotemporal resolution, as well obtain information on binding kinetics. A recent review[209] was focused on emerging applications of plasmonic scattering microscopy for single-protein imaging and single-cell analysis. As one of examples, nanofluidic scattering microscopy was applied for SMD in ref. 212.

Another important method for SMD is based on interferometric scattering microscopy (iSCAT), which is an extremely sensitive technique due to the combination of two factors: the ability to detect weak signals and the ability to separate these signals from a background.[210] Interferometric scattering microscopy can be used for high-speed single particle tracking, quantitative single-molecule characterization, and measurements of bio-molecular kinetics. It was shown that with the help of iSCAT one can obtain a high signal-to-noise ratio visualization of assemblies of biological materials such as proteins and lipids without the need for labels. It was also recently shown that iSCAT could become a promising tool for elucidating bio-molecular mechanisms on the plasma membrane.[213,214]

At the end of this section, we note that while applications of the microscopy methods for SMD requires a high-tech equipment, one could imagine their broader usage in a near future as microscopy can be implemented in extremely small volumes (as Leeuwenhoek showed in XVII century).

9. Current challenges and future perspectives of label-free ultrasensitive plasmonic biosensors

Newly-emerging optical biosensors based on new structural architectures and new materials, including emerging metamaterials, hybrid plasmonic-2D metasurfaces, metal/dielectric nanostructures, all-dielectric metasurfaces, are capable of generating a variety of novel phenomena, which can be employed to radically upgrade the sensitivity of current label-free biosensing technology and offer new attractive functionalities (imaging and multi-sensing option, superresolution, spectral tuneability, size selectivity, new functionalization strategies, *etc.*). In particular, designed plasmonic metamaterials open access to unprecedented ag mm^{-2} levels of areal mass sensitivity[33] and in some cases the reported LOD values were 3 orders of magnitude lower compared to all existing label-free and label-based biosensing methods.[38] The use of metamaterial-based architectures in combination with phase interrogation looks especially promising as it can lead to much lower limits of detection for a variety of small molecular weight analytes, see Fig. 2. At the same time, a great progress was achieved in dielectric biosensing platforms and platforms based on bound states in continuum and exceptional points. Extremely low LOD was reported for the biosensors based on the Goos–Hänchen effect and hyperbolic metamaterials.

Despite their extremely appealing characteristics, newly-emerging optical label-free technologies still require further instrumental elaboration and adaptation for concrete tasks of biomedical research. Current challenges and opportunities include the following:

1. The discussed label-free optical biosensing methods and metamaterial-based architectures can indeed provide an unprecedented improvement in the sensitivity of optical label-free biosensing, reaching the level of label methods (or better). However, high sensitivity often comes at the price of a limited dynamic range. Fortunately, as shown in ref. 38, even in the case of a very narrow dynamic range (*e.g.*, conditioned by a limited phase jump in phase-sensitive interrogation), a binding event can be accurately resolved by applying appropriate averaging and filtering algorithms. The limited dynamic range problem can be also tackled by employing feedback loops to keep the system within the range of maximal phase variation and/or by using additional signal recording channels.

2. An obstacle for the wide application of metamaterial-based sensor technology is related to the relative complexity of optical measurement instrumentation. For *en masse* applications, sensors should be based on inexpensive, robust and ready-to-use optical designs. We believe that some of the

discussed designs can indeed be compact and mobile, and can be used at the point-of-action or even at homes. As examples, one can imagine the development of miniaturized designs based on planar and fiber waveguide couplers,[103,106,107] compact integrated SPR interferometers[104] and Si-based integrating optics.[108,109] In future, new biosensor layouts could be incorporated in mobile phones,[110] which have the architecture necessary to perform optical biosensing provided the functionalized biosensing chips are available.

3. The development of low-cost and robust sensor transducers presents another important challenge. In this respect, Fourier nano-transducers and topologically dark metamaterials may have the edge from the point-of-view of simplicity and robustness, as they do not depend on local imperfections or structural non-uniformities. On the other hand, the low-cost fabrication of slides with the optical biochips is challenging. However, we believe that the problem could be solved by the development and adaptation of low-cost and scalable methods, including laser ablation (see an example in ref. 215), self-assembly or inkjet printing.

4. Functionalization is an essential part of any selective biosensing. Modern label-free optical sensors rely on bio-functionalization of gold. The surface of gold looks advantageous as the surface chemistry of gold is straightforward, while functionalization protocols are well developed for a variety of molecules used in biosensing. At the same time, 2D materials provide an excellent opportunity for bio-functionalization, especially in hybrid platforms, which combine 2D materials with conventional metal plasmonics. Recently, the protection of copper and silver plasmonics with 2D materials was demonstrated,[34] which led to the development of the layered material platform for biosensing.[60] In this platform, graphene-based surfaces allow the selective absorption of some molecules through pi-stacking forces, which opens up new avenues in bio-functionalization which is refreshingly different from gold bio-functionalization and allows the study of aromatic rings in bio-objects such as DNA, RNA, peptides, and cytokines.[35]

5. Last but not least, 2D atomic materials possess natural plasmons and phonon-polaritons which can provide sharp resonances useful for biosensing.[126,216] The main attraction of these resonances comes from the fact that they have frequencies overlapping with vibrational frequencies of biomolecules. Hence, in addition to detecting refractive index changes near nano-resonators, natural plasmons in 2D materials can also provide selectivity of detection without any use of functionalization through measuring subtle changes of resonant infrared spectra.[126,216] This attractive feature could lead to new biosensing platforms and the possibilities of biosensing provided by flat optics are still to be explored.

To conclude, there exist methods and architectures that provide unrivalled sensitivity of optical label-free biosensing that go well beyond the limits of detection of standard SPR and LPR platforms. We believe that future of label-free optical biosensing lies with simple, yet ingenious metamaterials (*e.g.*, Fourier nano-transducers/diffractive nonlocal media) which would guarantee quantitative point-of-care or point-of-action biosensing from simple unobtrusive test.

Author contributions

A. V. K. and A. N. G. conceived this review article and planned its content. A. V. K., V. G. K. and A. N. G. carried out an extensive research and analysis of the literature related to the subject, and wrote different parts of the manuscript. A. V. K. and A. N. G. assembled all parts and formulated the main ideas of the manuscript. All authors worked on the revised version of the article. A. V. K. and A. N. G. guided the project.

Conflicts of interest

There are no conflicts to declare.

Acknowledgements

AVK acknowledges financial support of the CNRS-DRI International Research Project (IRP) ''MINOS'' ANG and VGK acknowledge the support of Graphene Flagship Grant, Core 3 (881603). The authors also thank Prof. Irina Grigorieva for her invaluable help in preparing the manuscript.

References

1 F.-G. Banica, *Chemical Sensors and Biosensors: Fundamentals and Applications*, John Wiley & Sons, 2012.
2 M. A. Cooper, *Nat. Rev. Drug Discovery*, 2002, **1**, 515–528.
3 J. Kim, A. S. Campbell, B. E.-F. de Ávila and J. Wang, *Nat. Biotechnol.*, 2019, **37**, 389–406.
4 B. D. Malhotra and A. Chaubey, *Sens. Actuators, B*, 2003, **91**, 117–127.
5 G. Gauglitz, A. Brecht, G. Kraus and W. Mahm, *Sens. Actuators, B*, 1993, **11**, 21–27.
6 H. J. Watts, C. R. Lowe and D. V. Pollard-Knight, *Anal. Chem.*, 1994, **66**, 2465–2470.
7 C. Stamm and W. Lukosz, *Sens. Actuators, B*, 1994, **18**, 183–187.
8 S. Patskovsky, M. Meunier and A. V. Kabashin, *Opt. Express*, 2007, **15**, 12523–12528.
9 F. Vollmer and S. Arnold, *Nat. Methods*, 2008, **5**, 591–596.
10 B. Liedberg, C. Nylander and I. Lunström, *Sens. Actuators*, 1983, **4**, 299–304.
11 B. Liedberg, C. Nylander and I. Lundström, *Biosens. Bioelectron.*, 1995, **10**, i–ix.
12 J. Homola, *Anal. Bioanal. Chem.*, 2003, **377**, 528–539.
13 J. Homola, *Chem. Rev.*, 2008, **108**, 462–493.
14 R. B. M. E. Schasfoort, *Handbook of Surface Plasmon Resonance*, Royal Society of Chemistry, 2017.
15 J. N. Anker, W. P. Hall, O. Lyandres, N. C. Shah, J. Zhao and R. P. Van Duyne, *Nat. Mater.*, 2008, **7**, 442–453.
16 V. M. Agranovich and D. L. Mills, *Surface polaritons*, North-Holland, Amsterdam, 1982.
17 B. Špačková, P. Wrobel, M. Bocková and J. Homola, *Proc. IEEE*, 2016, **104**, 2380–2408.
18 Y. Xu, P. Bai, X. Zhou, Y. Akimov, C. E. Png, L.-K. Ang, W. Knoll and L. Wu, *Adv. Opt. Mater.*, 2019, **7**, 1801433.

19 X. Ma and S. J. Sim, *J. Mater. Chem. B*, 2020, **8**, 6197–6216.
20 A. Ahmadivand and B. Gerislioglu, *Laser Photonics Rev.*, 2022, **16**, 2100328.
21 J. Qin, S. Jiang, Z. Wang, X. Cheng, B. Li, Y. Shi, D. P. Tsai, A. Q. Liu, W. Huang and W. Zhu, *ACS Nano*, 2022, **16**, 11598–11618.
22 J.-H. Qu, A. Dillen, W. Saeys, J. Lammertyn and D. Spasic, *Anal. Chim. Acta*, 2020, **1104**, 10–27.
23 A. N. Grigorenko, P. I. Nikitin and A. V. Kabashin, *Appl. Phys. Lett.*, 1999, **75**, 3917–3919.
24 A. V. Kabashin, S. Patskovsky and A. N. Grigorenko, *Opt. Express*, 2009, **17**, 21191–21204.
25 A. V. Kabashin and P. I. Nikitin, *Quantum Electron.*, 1997, **27**, 653–654.
26 A. V. Kabashin and P. I. Nikitin, *Opt. Commun.*, 1998, **150**, 5–8.
27 H. P. Ho and W. W. Lam, *Sens. Actuators, B*, 2003, **96**, 554–559.
28 Y. Xinglong, W. Dingxin, W. Xing, D. Xiang, L. Wei and Z. Xinsheng, *Sens. Actuators, B*, 2005, **108**, 765–771.
29 Y. H. Huang, H. P. Ho, S. K. Kong and A. V. Kabashin, *Ann. Phys.*, 2012, **524**, 637–662.
30 A. G. Brolo, R. Gordon, B. Leathem and K. L. Kavanagh, *Langmuir*, 2004, **20**, 4813–4815.
31 A. V. Kabashin, P. Evans, S. Pastkovsky, W. Hendren, G. A. Wurtz, R. Atkinson, R. Pollard, V. A. Podolskiy and A. V. Zayats, *Nat. Mater.*, 2009, **8**, 867–871.
32 V. G. Kravets, F. Schedin, A. V. Kabashin and A. N. Grigorenko, *Opt. Lett.*, 2010, **35**, 956–958.
33 V. G. Kravets, F. Schedin, R. Jalil, L. Britnell, R. V. Gorbachev, D. Ansell, B. Thackray, K. S. Novoselov, A. K. Geim, A. V. Kabashin and A. N. Grigorenko, *Nat. Mater.*, 2013, **12**, 304–309.
34 V. G. Kravets, R. Jalil, Y. J. Kim, D. Ansell, D. E. Aznakayeva, B. Thackray, L. Britnell, B. D. Belle, F. Withers, I. P. Radko, Z. Han, S. I. Bozhevolnyi, K. S. Novoselov, A. K. Geim and A. N. Grigorenko, *Sci. Rep.*, 2014, **4**, 5517.
35 S. Zeng, K. V. Sreekanth, J. Shang, T. Yu, C.-K. Chen, F. Yin, D. Baillargeat, P. Coquet, H.-P. Ho, A. V. Kabashin and K.-T. Yong, *Adv. Mater.*, 2015, **27**, 6163–6169.
36 L. Malassis, P. Massé, M. Tréguer-Delapierre, S. Mornet, P. Weisbecker, P. Barois, C. R. Simovski, V. G. Kravets and A. N. Grigorenko, *Adv. Mater.*, 2014, **26**, 324–330.
37 K. V. Sreekanth, Y. Alapan, M. ElKabbash, E. Ilker, M. Hinczewski, U. A. Gurkan, A. De Luca and G. Strangi, *Nat. Mater.*, 2016, **15**, 621–627.
38 A. V. Kabashin, V. G. Kravets, F. Wu, S. Imaizumi, V. O. Shipunova, S. M. Deyev and A. N. Grigorenko, *Adv. Funct. Mater.*, 2019, **29**, 1902692.
39 M. Born and E. Wolf, *Principles of Optics*, Cambridge University Press, Cambridge, England, 1980.
40 V. G. Kravets, A. V. Kabashin, W. L. Barnes and A. N. Grigorenko, *Chem. Rev.*, 2018, **118**, 5912–5951.
41 V. G. Kravets, F. Schedin and A. N. Grigorenko, *Phys. Rev. Lett.*, 2008, **101**, 087403.
42 C. Cherqui, M. R. Bourgeois, D. Wang and G. C. Schatz, *Acc. Chem. Res.*, 2019, **52**, 2548–2558.
43 A. D. Utyushev, V. I. Zakomirnyi and I. L. Rasskazov, *Rev. Phys.*, 2021, **6**, 100051.
44 G. A. J. Besselink, R. P. H. Kooyman, P. J. H. J. van Os, G. H. M. Engbers and R. B. M. Schasfoort, *Anal. Biochem.*, 2004, **333**, 165–173.
45 J. Wang, Y. Luo, B. Zhang, M. Chen, J. Huang, K. Zhang, W. Gao, W. Fu, T. Jiang and P. Liao, *J. Transl. Med.*, 2011, **9**, 85.
46 H. Vaisocherová, K. Mrkvová, M. Piliarik, P. Jinoch, M. Steinbachová and J. Homola, *Biosens. Bioelectron.*, 2007, **22**, 1020–1026.
47 M. Bocková, X. Chadtová Song, E. Gedeonová, K. Levová, M. Kalousová, T. Zima and J. Homola, *Anal. Bioanal. Chem.*, 2016, **408**, 7265–7269.
48 D. Kotlarek, F. Curti, M. Vorobii, R. Corradini, M. Careri, W. Knoll, C. Rodriguez-Emmenegger and J. Dostálek, *Sens. Actuators, B*, 2020, **320**, 128380.
49 S.-P. Ng, C.-M. L. Wu, S.-Y. Wu, H.-P. Ho and S. K. Kong, *Biosens. Bioelectron.*, 2010, **26**, 1593–1598.
50 Y.-C. Li, Y.-F. Chang, L.-C. Su and C. Chou, *Anal. Chem.*, 2008, **80**, 5590–5595.
51 T. J. Park, S. J. Lee, D. K. Kim, N. S. Heo, J. Y. Park and S. Y. Lee, *Talanta*, 2012, **89**, 246–252.
52 W.-J. Zhou, A. R. Halpern, T. H. Seefeld and R. M. Corn, *Anal. Chem.*, 2012, **84**, 440–445.
53 F. Wu, J. Singh, P. A. Thomas, Q. Ge, V. G. Kravets, P. J. Day and A. N. Grigorenko, *2D Mater.*, 2020, **7**, 045019.
54 H. Jiang, T. Li, E. Ertorer, J. Yang, J. Sabarinathan and S. Mittler, *Sens. Actuators, A*, 2013, **189**, 474–480.
55 M. K. Kang, J. Lee, A. H. Nguyen and S. J. Sim, *Biosens. Bioelectron.*, 2015, **72**, 197–204.
56 J. Ozhikandathil, S. Badilescu and M. Packirisamy, *J. Biomed. Opt.*, 2012, **17**, 077001.
57 Y. Shen, J. Zhou, T. Liu, Y. Tao, R. Jiang, M. Liu, G. Xiao, J. Zhu, Z.-K. Zhou, X. Wang, C. Jin and J. Wang, *Nat. Commun.*, 2013, **4**, 2381.
58 M. Piliarik, H. Šípová, P. Kvasnička, N. Galler, J. R. Krenn and J. Homola, *Opt. Express*, 2012, **20**, 672–680.
59 G. Qiu, S. P. Ng and L. C.-M. Wu, *Sens. Actuators, B*, 2016, **234**, 247–254.
60 F. Wu, P. A. Thomas, V. G. Kravets, H. O. Arola, M. Soikkeli, K. Iljin, G. Kim, M. Kim, H. S. Shin, D. V. Andreeva, C. Neumann, M. Küllmer, A. Turchanin, D. De Fazio, O. Balci, V. Babenko, B. Luo, I. Goykhman, S. Hofmann, A. C. Ferrari, K. S. Novoselov and A. N. Grigorenko, *Sci. Rep.*, 2019, **9**, 20286.
61 K. V. Sreekanth, S. Sreejith, Y. Alapan, M. Sitti, C. T. Lim and R. Singh, *Adv. Opt. Mater.*, 2019, **7**, 1801313.
62 K. V. Sreekanth, Q. Ouyang, S. Sreejith, S. Zeng, W. Lishu, E. Ilker, W. Dong, M. ElKabbash, Y. Ting and C. T. Lim, *Adv. Opt. Mater.*, 2019, **7**, 1900081.
63 A. N. Grigorenko, A. K. Geim, H. F. Gleeson, Y. Zhang, A. A. Firsov, I. Y. Khrushchev and J. Petrovic, *Nature*, 2005, **438**, 335–338.
64 R. Azzam and N. Bashara, *Ellipsometry and Polarized Light*, North-Holland, Amsterdam, 1977.

65 S. Hénon and J. Meunier, *Rev. Sci. Instrum.*, 1991, **62**, 936–939.
66 M. R. Dennis, K. O'Holleran and M. J. Padgett, in *Progress in Optics*, ed. E. Wolf, Elsevier, 2009, vol. 53, pp. 293–363.
67 T. Turbadar, *Proc. Phys. Soc.*, 1959, **73**, 40–44.
68 V. G. Kravets, F. Schedin and A. N. Grigorenko, *Phys. Rev. B: Condens. Matter Mater. Phys.*, 2008, **78**, 205405.
69 M. A. Kats, D. Sharma, J. Lin, P. Genevet, R. Blanchard, Z. Yang, M. M. Qazilbash, D. N. Basov, S. Ramanathan and F. Capasso, *Appl. Phys. Lett.*, 2012, **101**, 221101.
70 G. Ermolaev, K. Voronin, D. G. Baranov, V. Kravets, G. Tselikov, Y. Stebunov, D. Yakubovsky, S. Novikov, A. Vyshnevyy, A. Mazitov, I. Kruglov, S. Zhukov, R. Romanov, A. M. Markeev, A. Arsenin, K. S. Novoselov, A. N. Grigorenko and V. Volkov, *Nat. Commun.*, 2022, **13**, 2049.
71 P. A. Thomas, K. S. Menghrajani and W. L. Barnes, *Nat. Commun.*, 2022, **13**, 1809.
72 M. S. Ergoktas, S. Soleymani, N. Kakenov, K. Wang, T. B. Smith, G. Bakan, S. Balci, A. Principi, K. S. Novoselov, S. K. Ozdemir and C. Kocabas, *Science*, 2022, **376**, 184–188.
73 A. Berkhout and A. F. Koenderink, *ACS Photonics*, 2019, **6**, 2917–2925.
74 C. A. Dennett, N. Poudel, P. J. Simmonds, A. Tiwari, D. H. Hurley and K. Gofryk, *Nat. Commun.*, 2022, **13**, 2221.
75 F. Yesilkoy, R. A. Terborg, J. Pello, A. A. Belushkin, Y. Jahani, V. Pruneri and H. Altug, *Light: Sci. Appl.*, 2018, **7**, 17152.
76 F. Abelès, *Surf. Sci.*, 1976, **56**, 237–251.
77 S. Y. Wu, H. P. Ho, W. C. Law, C. Lin and S. K. Kong, *Opt. Lett.*, 2004, **29**, 2378–2380.
78 H.-P. Chiang, J.-L. Lin and Z.-W. Chen, *Appl. Phys. Lett.*, 2006, **88**, 141105.
79 S. Patskovsky, M. Meunier, P. N. Prasad and A. V. Kabashin, *Opt. Express*, 2010, **18**, 14353–14358.
80 M. Kashif, A. A. Bakar, N. Arsad and S. Shaari, *Sensors*, 2014, **14**, 15914–15938.
81 S. Deng, P. Wang and X. Yu, *Sensors*, 2017, **17**, 2819.
82 F. Sohrabi, S. Saeidifard and S. M. Hamidi, *Opt. Quantum Electron.*, 2021, **53**, 710.
83 R. Naraoka and K. Kajikawa, *Sens. Actuators, B*, 2005, **107**, 952–956.
84 S. Patskovsky, R. Jacquemart, M. Meunier, G. De Crescenzo and A. V. Kabashin, *Sens. Actuators, B*, 2008, **133**, 628–631.
85 I. R. Hooper and J. R. Sambles, *Appl. Phys. Lett.*, 2004, **85**, 3017–3019.
86 H. P. Ho, W. C. Law, S. Y. Wu, X. H. Liu, S. P. Wong, C. Lin and S. K. Kong, *Sens. Actuators, B*, 2006, **114**, 80–84.
87 P. P. Markowicz, W. C. Law, A. Baev, P. N. Prasad, S. Patskovsky and A. V. Kabashin, *Opt. Express*, 2007, **15**, 1745–1754.
88 W.-C. Law, P. Markowicz, K.-T. Yong, I. Roy, A. Baev, S. Patskovsky, A. V. Kabashin, H.-P. Ho and P. N. Prasad, *Biosens. Bioelectron.*, 2007, **23**, 627–632.
89 A. V. Kabashin, V. E. Kochergin, A. A. Beloglazov and P. I. Nikitin, *Biosens. Bioelectron.*, 1998, **13**, 1263–1269.
90 A. V. Kabashin, V. E. Kochergin and P. I. Nikitin, *Sens. Actuators, B*, 1999, **54**, 51–56.
91 J. Homola and S. S. Yee, *Sens. Actuators, B*, 1998, **51**, 331–339.
92 A. N. Grigorenko, A. A. Beloglazov, P. I. Nikitin, C. Kuhne, G. Steiner and R. Salzer, *Opt. Commun.*, 2000, **174**, 151–155.
93 M. Piliarik and J. Homola, *Sens. Actuators, B*, 2008, **134**, 353–355.
94 K. Thadson, S. Visitsattapongse and S. Pechprasarn, *Sci. Rep.*, 2021, **11**, 1–14.
95 S. G. Nelson, K. S. Johnston and S. S. Yee, *Sens. Actuators, B*, 1996, **35**, 187–191.
96 W. Yuan, H. P. Ho, C. L. Wong, S. K. Kong and C. Lin, *IEEE Sens. J.*, 2007, **7**, 70–73.
97 H. P. Ho, W. Yuan, C. L. Wong, S. Y. Wu, Y. K. Suen, S. K. Kong and C. Lin, *Opt. Commun.*, 2007, **275**, 491–496.
98 Y. D. Su, S. J. Chen and T. L. Yeh, *Opt. Lett.*, 2005, **30**, 1488–1490.
99 C. L. Wong, H. P. Ho, Y. K. Suen, S. K. Kong, Q. L. Chen, W. Yuan and S. Y. Wu, *Biosens. Bioelectron.*, 2008, **24**, 606–612.
100 M. G. Somekh, G. Stabler, S. Liu, J. Zhang and C. W. See, *Opt. Lett.*, 2009, **34**, 3110–3112.
101 Y. H. Huang, H. P. Ho, S. Y. Wu, S. K. Kong, W. W. Wong and P. Shum, *Opt. Lett.*, 2011, **36**, 4092–4094.
102 R. Wang, C. Zhang, Y. Yang, S. Zhu and X. C. Yuan, *Opt. Lett.*, 2012, **37**, 2091–2093.
103 A. K. Sheridan, R. D. Harris, P. N. Bartlett and J. S. Wilkinson, *Sens. Actuators, B*, 2004, **97**, 114–121.
104 P. Debackere, S. Scheerlinck, P. Bienstman and R. Baets, *Opt. Express*, 2007, **15**, 13651–13653.
105 M. Hedhly, Y. Wang, S. Zeng, F. Ouerghi, J. Zhou and G. Humbert, *Biosensors*, 2022, **12**, 457.
106 G. Nemova, A. V. Kabashin and R. Kashyap, *J. Opt. Soc. Am. B*, 2008, **25**, 1673–1677.
107 A. Hassani, B. Gauvreau, M. F. Fehri, A. Kabashin and M. Skorobogatiy, *Electromagnetics*, 2008, **28**, 198–213.
108 S. Patskovsky, A. V. Kabashin, M. Meunier and J. H. T. Luong, *Appl. Opt.*, 2003, **42**, 6905–6909.
109 S. Patskovsky, A. V. Kabashin, M. Meunier and J. H. T. Luong, *Sens. Actuators, B*, 2004, **97**, 409–414.
110 Y. Liu, Q. Liu, S. Chen, F. Cheng, H. Wang and W. Peng, *Sci. Rep.*, 2015, **5**, 12864.
111 Z. L. Cao, S. L. Wong, S. Y. Wu, H. P. Ho and H. C. Ong, *Appl. Phys. Lett.*, 2014, **104**, 171116.
112 S. H. Lee, N. C. Lindquist, N. J. Wittenberg, L. R. Jordan and S.-H. Oh, *Lab Chip*, 2012, **12**, 3882–3890.
113 W.-C. Law, K.-T. Yong, A. Baev, R. Hu and P. N. Prasad, *Opt. Express*, 2009, **17**, 19041–19046.
114 W.-C. Law, K.-T. Yong, A. Baev and P. N. Prasad, *ACS Nano*, 2011, **5**, 4858–4864.
115 X. Zhao, T. Huang, S. Zeng, C. Song, Z. Cheng, X. Wu, P. Huang, J. Pan, Y. Wu and P. P. Shum, *Plasmonics*, 2020, **15**, 769–781.
116 G. Qiu, S. P. Ng and C.-M. L. Wu, *Biosens. Bioelectron.*, 2018, **106**, 129–135.

117 R. S. Moirangthem, M. T. Yaseen, P. K. Wei, J. Y. Cheng and Y. C. Chang, *Biomed. Opt. Express*, 2012, **3**, 899–910.
118 K. Lodewijks, W. Van Roy, G. Borghs, L. Lagae and P. Van Dorpe, *Nano Lett.*, 2012, **12**, 1655–1659.
119 R. S. Moirangthem, Y. C. Chang and P. K. Wei, *Opt. Lett.*, 2011, **36**, 775–777.
120 M. Svedendahl, R. Verre and M. Käll, *Light: Sci. Appl.*, 2014, **3**, e220.
121 G. Qiu, S. P. Ng and C. M. L. Wu, *Opt. Lett.*, 2015, **40**, 1924–1927.
122 A. Thakur, G. Qiu, S.-P. Ng, J. Guan, J. Yue, Y. Lee and C.-M. L. Wu, *Biosens. Bioelectron.*, 2017, **94**, 400–407.
123 A. K. Geim and K. S. Novoselov, *Nat. Mater.*, 2007, **6**, 183–191.
124 S. Szunerits, N. Maalouli, E. Wijaya, J.-P. Vilcot and R. Boukherroub, *Anal. Bioanal. Chem.*, 2013, **405**, 1435–1443.
125 A. N. Grigorenko, M. Polini and K. S. Novoselov, *Nat. Photonics*, 2012, **6**, 749–758.
126 D. Rodrigo, O. Limaj, D. Janner, D. Etezadi, F. J. García de Abajo, V. Pruneri and H. Altug, *Science*, 2015, **349**, 165.
127 P. Subramanian, A. Lesniewski, I. Kaminska, A. Vlandas, A. Vasilescu, J. Niedziolka-Jonsson, E. Pichonat, H. Happy, R. Boukherroub and S. Szunerits, *Biosens. Bioelectron.*, 2013, **50**, 239–243.
128 S. Zeng, S. Hu, J. Xia, T. Anderson, X.-Q. Dinh, X.-M. Meng, P. Coquet and K.-T. Yong, *Sens. Actuators, B*, 2015, **207**, 801–810.
129 S. P. Ng, G. Qiu, N. Ding, X. Lu and C.-M. L. Wu, *Biosens. Bioelectron.*, 2017, **89**, 468–476.
130 N.-F. Chiu, T.-L. Lin and C.-T. Kuo, *Sens. Actuators, B*, 2018, **265**, 264–272.
131 V. G. Kravets, F. Wu, T. Yu and A. N. Grigorenko, *Plasmonics*, 2022, **17**, 973–987.
132 Y. Wang, S. Zeng, A. Crunteanu, Z. Xie, G. Humbert, L. Ma, Y. Wei, A. Brunel, B. Bessette, J.-C. Orlianges, F. Lalloué, O. G. Schmidt, N. Yu and H.-P. Ho, *Nano-Micro Lett.*, 2021, **13**, 96.
133 S. Rossi, E. Gazzola, P. Capaldo, G. Borile and F. Romanato, *Sensors*, 2018, **18**, 1621.
134 P. Bouchal, P. Dvořák, J. Babocký, Z. Bouchal, F. Ligmajer, M. Hrtoň, V. Křápek, A. Faßbender, S. Linden, R. Chmelík and T. Šikola, *Nano Lett.*, 2019, **19**, 1242–1250.
135 A. S. Kushwaha, A. Kumar, R. Kumar and S. K. Srivastava, *Photonics and Nanostructures - Fundamentals and Applications*, 2018, **31**, 99–106.
136 Q. Ouyang, S. Zeng, L. Jiang, J. Qu, X.-Q. Dinh, J. Qian, S. He, P. Coquet and K.-T. Yong, *J. Phys. Chem. C*, 2017, **121**, 6282–6289.
137 L. Han, Z. Chen, T. Huang, H. Ding and C. Wu, *Plasmonics*, 2020, **15**, 693–701.
138 P. Varasteanu, *Plasmonics*, 2020, **15**, 243–253.
139 X. Zhao, T. Huang, P. S. Ping, X. Wu, P. Huang, J. Pan, Y. Wu and Z. Cheng, *Sensors*, 2018, **18**, 2056.
140 T. Yang and H. P. Ho, *Opt. Express*, 2009, **17**, 11205–11216.
141 H. K. Baghbadorani, J. Barvestani and S. R. Entezar, *Appl. Opt.*, 2017, **56**, 462–469.
142 J. Tong, L. Jiang, H. Chen, Y. Wang, K.-T. Yong, E. Forsberg and S. He, *Opt. Commun.*, 2018, **410**, 817–823.
143 T. Huang, S. Zeng, X. Zhao, Z. Cheng and P. Shum, *Photonics*, 2018, **5**, 23.
144 Y. Li, Y. Yuan, X. Peng, J. Song, J. Liu and J. Qu, *RSC Adv.*, 2019, **9**, 29805–29812.
145 L. Han, X. Zhao, T. Huang, H. Ding and C. Wu, *Plasmonics*, 2019, **14**, 1743–1750.
146 Y. Tsurimaki, J. K. Tong, V. N. Boriskin, A. Semenov, M. I. Ayzatsky, Y. P. Machekhin, G. Chen and S. V. Boriskina, *ACS Photonics*, 2018, **5**, 929–938.
147 U. Laor and G. C. Schatz, *Chem. Phys. Lett.*, 1981, **82**, 566–570.
148 S. Zou, N. Janel and G. C. Schatz, *J. Chem. Phys.*, 2004, **120**, 10871–10875.
149 P. Nordlander, C. Oubre, E. Prodan, K. Li and M. I. Stockman, *Nano Lett.*, 2004, **4**, 899–903.
150 B. Thackray, V. G. Kravets, F. Schedin, R. Jalil and A. N. Grigorenko, *J. Opt.*, 2013, **15**, 114002.
151 P. Chandra, Y. N. Tan and S. P. Singh, *Next generation point-of-care biomedical sensors technologies for cancer diagnosis*, Springer, 2017.
152 K. V. Sreekanth, Q. Ouyang, S. Sreejith, S. Zeng, W. Lishu, E. Ilker, W. Dong, M. ElKabbash, Y. Ting, C. T. Lim, M. Hinczewski, G. Strangi, K.-T. Yong, R. E. Simpson and R. Singh, *Adv. Opt. Mater.*, 2019, **7**, 1900081.
153 G. Strangi, K. V. Sreekanth and M. Elkabbash, in *Next Generation Point-of-care Biomedical Sensors Technologies for Cancer Diagnosis*, ed. P. Chandra, Y. N. Tan and S. P. Singh, Springer Singapore, Singapore, 2017, pp. 155–172, DOI: 10.1007/978-981-10-4726-8_7.
154 M. S. Bin-Alam, O. Reshef, Y. Mamchur, M. Z. Alam, G. Carlow, J. Upham, B. T. Sullivan, J.-M. Ménard, M. J. Huttunen and R. W. Boyd, *Nat. Commun.*, 2021, **12**, 1–8.
155 J. Wu, F. Wu, C. Xue, Z. Guo, H. Jiang, Y. Sun, Y. Li and H. Chen, *Opt. Express*, 2019, **27**, 24835–24846.
156 L. Wang, Q. Wang, T.-Q. Wang, W.-M. Zhao, X.-Y. Yin, J.-X. Jiang and S.-S. Zhang, *Nanoscale*, 2022, **14**, 6144–6151.
157 A. Danilov, G. Tselikov, F. Wu, V. G. Kravets, I. Ozerov, F. Bedu, A. N. Grigorenko and A. V. Kabashin, *Biosens. Bioelectron.*, 2018, **104**, 102–112.
158 X. Yang, L. Xiong, Y. Lu and G. Li, *J. Phys. D: Appl. Phys.*, 2020, **53**, 465109.
159 I. Barth, D. Conteduca, C. Reardon, S. Johnson and T. F. Krauss, *Light: Sci. Appl.*, 2020, **9**, 96.
160 A. Overvig and A. Alù, *Laser Photonics Rev.*, 2022, 2100633.
161 H. Song, N. Zhang, J. Duan, Z. Liu, J. Gao, M. H. Singer, D. Ji, A. R. Cheney, X. Zeng, B. Chen, S. Jiang and Q. Gan, *Adv. Opt. Mater.*, 2017, **5**, 1700166.
162 C. Coutant, S. Ravaine, X. Wang, J. Toudert, V. Ponsinet and P. Barois, *Rendiconti Lincei*, 2015, **26**, 175–182.
163 A. I. Aristov, M. Manousidaki, A. Danilov, K. Terzaki, C. Fotakis, M. Farsari and A. V. Kabashin, *Sci. Rep.*, 2016, **6**, 1–8.
164 K. V. Sreekanth, S. Sreejith, S. Han, A. Mishra, X. Chen, H. Sun, C. T. Lim and R. Singh, *Nat. Commun.*, 2018, **9**, 369.

165 V. Sreekanth, M. ElKabbash, V. Caligiuri, R. Singh, A. De Luca and G. Strangi, *New Directions in Thin Film Nanophotonics*, Springer Singapore, 2019.
166 L. Jiang, S. Zeng, Z. Xu, Q. Ouyang, D. H. Zhang, P. H. J. Chong, P. Coquet, S. He and K. T. Yong, *Small*, 2017, **13**, 1700600.
167 Y. Zou, Y. Liu and G. Song, *Sensors*, 2022, **22**, 2116.
168 F. Goos and H. Hänchen, *Ann. Phys.*, 1947, **436**, 333–346.
169 F. Goos and H. Lindberg-Hänchen, *Ann. Phys.*, 1949, **440**, 251–252.
170 X. Yin, L. Hesselink, Z. Liu, N. Fang and X. Zhang, *Appl. Phys. Lett.*, 2004, **85**, 372–374.
171 R.-G. Wan and M. S. Zubairy, *Opt. Express*, 2020, **28**, 6036–6047.
172 Z. Qin, C. Yue, Y. Lang and Q. Liu, *Opt. Commun.*, 2018, **426**, 16–22.
173 Z. Liu, F. Lu, L. Jiang, W. Lin and Z. Zheng, *Biosensors*, 2021, **11**, 201.
174 S. Zeng, G. Liang, A. Gheno, S. Vedraine, B. Ratier, H.-P. Ho and N. Yu, *Nanomaterials*, 2020, **10**, 1289.
175 Q. You, Y. Shan, S. Gan, Y. Zhao, X. Dai and Y. Xiang, *Opt. Mater. Express*, 2018, **8**, 3036–3048.
176 L. Han, J. Pan, C. Wu, K. Li, H. Ding, Q. Ji, M. Yang, J. Wang, H. Zhang and T. Huang, *Sensors*, 2020, **20**, 1028.
177 K. V. Sreekanth, Q. Ouyang, S. Han, K.-T. Yong and R. Singh, *Appl. Phys. Lett.*, 2018, **112**, 161109.
178 C.-W. Chang, X. Xu, S. Chakravarty, H.-C. Huang, L.-W. Tu, Q. Y. Chen, H. Dalir, M. A. Krainak and R. T. Chen, *Biosens. Bioelectron.*, 2019, **141**, 111396.
179 K. V. Sreekanth, W. Dong, Q. Ouyang, S. Sreejith, M. ElKabbash, C. T. Lim, G. Strangi, K.-T. Yong, R. E. Simpson and R. Singh, *ACS Appl. Mater. Interfaces*, 2018, **10**, 34991–34999.
180 A. B. Evlyukhin, S. M. Novikov, U. Zywietz, R. L. Eriksen, C. Reinhardt, S. I. Bozhevolnyi and B. N. Chichkov, *Nano Lett.*, 2012, **12**, 3749–3755.
181 A. I. Kuznetsov, A. E. Miroshnichenko, M. L. Brongersma, Y. S. Kivshar and B. Luk'yanchuk, *Science*, 2016, **354**, aag2472.
182 S. Kruk and Y. Kivshar, *ACS Photonics*, 2017, **4**, 2638–2649.
183 C. F. Bohren and D. R. Huffman, *Absorption and scattering of light by small particles*, John Wiley & Sons, 2008.
184 N. Bontempi, K. E. Chong, H. W. Orton, I. Staude, D.-Y. Choi, I. Alessandri, Y. S. Kivshar and D. N. Neshev, *Nanoscale*, 2017, **9**, 4972–4980.
185 O. Yavas, M. Svedendahl, P. Dobosz, V. Sanz and R. Quidant, *Nano Lett.*, 2017, **17**, 4421–4426.
186 M. L. Tseng, Y. Jahani, A. Leitis and H. Altug, *ACS Photonics*, 2020, **8**, 47–60.
187 R. A. Aoni, S. Manjunath, B. I. Karawdeniya, K. Zangeneh Kamali, L. Xu, A. M. Damry, C. J. Jackson, A. Tricoli, A. E. Miroshnichenko and M. Rahmani, *Adv. Funct. Mater.*, 2022, **32**, 2103143.
188 M. Iwanaga and W. Tangkawsakul, *Biosensors*, 2022, **12**, 981.
189 M. Iwanaga, *ACS Nano*, 2020, **14**, 17458–17467.
190 H. Altug, S.-H. Oh, S. A. Maier and J. Homola, *Nat. Nanotechnol.*, 2022, **17**, 5–16.
191 Z. Wang, J. Sun, J. Li, L. Wang, Z. Li, X. Zheng and L. Wen, *Adv. Sci.*, 2023, 2206236.
192 C. W. Hsu, B. Zhen, A. D. Stone, J. D. Joannopoulos and M. Soljačić, *Nat. Rev. Mater.*, 2016, **1**, 1–13.
193 K. Koshelev, A. Bogdanov and Y. Kivshar, *Sci. Bulletin*, 2019, **64**, 836–842.
194 J. v Neumann and E. Wigner, *Phys. Z.*, 1929, **30**, 291–293.
195 Y. Jahani, E. R. Arvelo, F. Yesilkoy, K. Koshelev, C. Cianciaruso, M. De Palma, Y. Kivshar and H. Altug, *Nat. Commun.*, 2021, **12**, 3246.
196 F. Wu, D. Liu and X. Yu, *Results Phys.*, 2023, 106539.
197 C. Schiattarella, G. Sanità, B. G. Alulema, V. Lanzio, S. Cabrini, A. Lamberti, I. Rendina, V. Mocella, G. Zito and S. Romano, *Biosens. Bioelectron.: X*, 2022, **12**, 100262.
198 G. Zito, G. Sanità, B. Guilcapi Alulema, S. N. Lara Yépez, V. Lanzio, F. Riminucci, S. Cabrini, M. Moccia, C. Avitabile and A. Lamberti, *Nanophotonics*, 2021, **10**, 4279–4287.
199 L. Kühner, L. Sortino, R. Berté, J. Wang, H. Ren, S. A. Maier, Y. Kivshar and A. Tittl, *Nat. Commun.*, 2022, **13**, 4992.
200 F. Yesilkoy, E. R. Arvelo, Y. Jahani, M. Liu, A. Tittl, V. Cevher, Y. Kivshar and H. Altug, *Nat. Photonics*, 2019, **13**, 390–396.
201 L. Feng, R. El-Ganainy and L. Ge, *Nat. Photonics*, 2017, **11**, 752–762.
202 M.-A. Miri and A. Alù, *Science*, 2019, **363**, eaar7709.
203 J. Wiersig, *Phys. Rev. Lett.*, 2014, **112**, 203901.
204 W. Chen, Ş. Kaya Özdemir, G. Zhao, J. Wiersig and L. Yang, *Nature*, 2017, **548**, 192–196.
205 S. H. Park, S. Xia, S.-H. Oh, P. Avouris and T. Low, *ACS Photonics*, 2021, **8**, 3241–3248.
206 B. Liu, S. Zhao, X. Chen, X. Zhou, H. Zhu, F. Wang, X. Yan, T. Cheng and X. Zhang, *IEEE Sens. J.*, 2023, **23**, 11662–11671.
207 Y. Liu, P. Yan, F. Liu, A. Jian and S. Sang, *Micromachines*, 2021, **12**, 426.
208 J.-H. Park, A. Ndao, W. Cai, L. Hsu, A. Kodigala, T. Lepetit, Y.-H. Lo and B. Kanté, *Nat. Phys.*, 2020, **16**, 462–468.
209 P. Zhang, X. Zhou and S. Wang, *Chem. Methods*, 2023, e202200066.
210 G. Young and P. Kukura, *Annu. Rev. Phys. Chem.*, 2019, **70**, 301–322.
211 P. Zhang, G. Ma, W. Dong, Z. Wan, S. Wang and N. Tao, *Nat. Methods*, 2020, **17**, 1010–1017.
212 B. Špačková, H. Klein Moberg, J. Fritzsche, J. Tenghamn, G. Sjösten, H. Šípová-Jungová, D. Albinsson, Q. Lubart, D. van Leeuwen and F. Westerlund, *Nat. Methods*, 2022, **19**, 751–758.
213 E. D. Foley, M. S. Kushwah, G. Young and P. Kukura, *Nat. Methods*, 2021, **18**, 1247–1252.
214 T. Heermann, F. Steiert, B. Ramm, N. Hundt and P. Schwille, *Nat. Methods*, 2021, **18**, 1239–1246.
215 A. I. Aristov, U. Zywietz, A. B. Evlyukhin, C. Reinhardt, B. N. Chichkov and A. V. Kabashin, *Appl. Phys. Lett.*, 2014, **104**, 071101.
216 M. Autore, P. Li, I. Dolado, F. J. Alfaro-Mozaz, R. Esteban, A. Atxabal, F. Casanova, L. E. Hueso, P. Alonso-González, J. Aizpurua, A. Y. Nikitin, S. Vélez and R. Hillenbrand, *Light: Sci. Appl.*, 2018, **7**, 17172.